Article

Not peer-reviewed version

Space as an Ether Crystal: A Unified Model of Gravity, Electromagnetism, Light, and Matter

Örs Márton *

Posted Date: 7 April 2026

doi: 10.20944/preprints202604.0421.v1

Keywords: superfluid vacuum theory; ether; FCC lattice; crowdion soliton; hyphon; hedron; emergent gravity; unified model; vortex model of matter; fine structure constant; electron delocalization; neutron charge distribution; rock salt ordering

 doi:10.20944/preprints202604.0421.v1

Article

Space as an Ether Crystal: A Unified Model of Gravity, Electromagnetism, Light, and Matter

Örs Márton

Independent Researcher, Hungary; marton_ors@yahoo.com

Abstract

Classical physics describes gravity, electromagnetism, and light with extraordinary precision but not what they are — this paper proposes a unified mechanical model: they are consequences of space being a crystal of spinning spheres. The elements of this crystal — called hyphons (from Greek hyphē, fabric) — are vortices in a superfluid ether, each spinning on one of four tetrahedral axes, packed in the same face-centred cubic (FCC) arrangement as the atoms in a silver crystal. Transverse sound travels through silver at 1,600 m/s — a wave governed by the lattice spacing, stiffness, and density. Light, in this model, is the same kind of wave in the hyphon crystal, governed by the same wave mechanics, travelling at the speed of light. The hyphon diameter is 0.105 fm, half the proton's reduced Compton wavelength. The crystal picture describes undisturbed space; where enough energy concentrates to disrupt the lattice — inside particles and black holes — the underlying superfluid nature of the medium becomes visible. The proton is approximately 1000 hyphons organised into a toroidal (doughnut-shaped) vortex, with a positron orbiting on its surface, giving it charge +1e. The neutron is the same vortex with an electron orbiting just above the surface, cancelling the charge. The electron itself is a different kind of excitation: when an extra atom is forced into a close-packed row of a crystal, it creates a propagating disturbance called a crowdion — a well-studied phenomenon in metals. Every proton and neutron is a vortex that creates a pressure drop propagating through the crystal as a 1/r field — this is gravity. The hyphons carry enormous base energy, but because it is perfectly uniform, only the excitations above it are visible as mass. Charge is lattice distortion: the crowdion disrupts the crystal at every position, producing a strain pattern that attracts opposite distortions and repels like ones. The strong nuclear force is surface contact energy between nucleon spheres in rock salt ordering. The weak nuclear force is the energy threshold for the electron to escape the neutron's surface orbit — beta decay. Inside nuclei, these electrons delocalize between proton cores. The fine structure constant is computed from the crystal's geometry and coupling parameters as $1/\alpha = 152$ (measured: 137).

Keywords: superfluid vacuum theory; ether; FCC lattice; crowdion soliton; hyphon; hedron; emergent gravity; unified model; vortex model of matter; fine structure constant; electron delocalization; neutron charge distribution; rock salt ordering

1. Introduction

Classical physics describes gravity, electromagnetism, and light with extraordinary precision but does not answer what they are. General relativity describes how mass curves spacetime but not what spacetime is. Maxwell's equations describe fields but not what a field is. This paper proposes that space is a crystal of spinning spheres — and that forces, light, and particles are mechanical consequences of this crystal's structure.

The closest familiar analogue is a metal. Silver has a face-centred cubic (FCC) crystal structure — atoms packed like cannonballs, each touching twelve neighbours. Transverse sound travels through silver at 1,600 m/s, a speed set not by individual atoms but by the lattice's spacing, stiffness, and density. In this model, light is the same kind of wave in the same kind of lattice, at a much smaller scale.

 doi:10.20944/preprints202604.0421.v1

The model begins with a single substance: the hedron (from Greek hedra, ἕδρα, meaning foundation) — the fundamental particle of the ether, whose size has not been determined. Hedrons organise into hyphons (from Greek hyphē, ὑφή, meaning fabric) — spinning spherical vortices of diameter 0.105 fm, each a self-sustaining circulation pattern in the hedron fluid. These hyphons are packed in FCC arrangement, and each spins on one of four tetrahedral axes, like four different orientations of spinning tops in a repeating pattern. This tetrahedral geometry guarantees that the speed of light is the same in all directions — not as a postulate, but as a mathematical identity: the total flywheel resistance from four tetrahedral axes sums to exactly 8/3 regardless of direction (Section 2.1). The hyphon diameter is half the proton's reduced Compton wavelength: $d = \hbar/(2m_pc)$, linking the lattice spacing directly to the proton mass (Section 2.3).

Calling space a crystal is precise for undisturbed space, but the hyphons are not static atoms — they are vortices in a superfluid. When enough energy concentrates in a region, the crystal lattice breaks down and the fluid nature becomes visible. This is how particles form. Consider water in a pool: calm and uniform until someone creates a vortex — a smoke ring or a bubble ring. The vortex is made of the same water but is a distinct structure with its own energy, shape, and persistence. In the hyphon lattice, the proton is such a vortex: approximately 1000 hyphons organised into a toroidal (doughnut-shaped) circulation pattern. Its mass — 938 MeV — is the energy cost of maintaining this circulation above the calm lattice ground state. This is demonstrated directly by neutral pion decay, where 100% of the mass radiates as photons: no special substance leaves, only the circulation energy is released (Section 5.2).

A positron orbits on the proton's surface, giving it charge +1e. The neutron is the same vortex with an additional electron orbiting just above the surface, cancelling the charge. How these structures are held together, and why the proton is stable while most other vortex configurations decay, is discussed in Section 5.2.

The electron is a fundamentally different kind of excitation. Imagine a row of balls packed tightly in a tube: push one extra ball in from the side. It has no room, so it shoves its neighbour, which shoves the next, and a compression pulse travels down the row. The balls themselves barely move, but the disturbance — the pattern — propagates at a speed set by the stiffness of the packing. In crystallography, this is called a crowdion: an extra atom in a close-packed row, travelling as a soliton. Crowdion propagation has been confirmed by molecular dynamics in FCC metals at speeds up to 11 km/s (Shepelev et al., 2023). Key properties of the crowdion — including relativistic dispersion and two mirror-image forms — correspond to known properties of the electron (Section 5.1).

The search for a mechanical medium for light dates to Fresnel (1818) and was largely abandoned after Michelson and Morley (1887) found no ether wind. But as Dirac (1951) argued, relativity does not rule out the ether — only a detectable rest frame. In this model, every measuring instrument is itself a pattern in the lattice, so Lorentz contraction and time dilation emerge as real mechanical effects that cancel any detection attempt (Section 3.4). This work builds upon Superfluid Vacuum Theory as developed by Volovik (2003), Zloshchastiev (2011), and others, extending it to concrete mechanical structures.

From the crystal structure and these two types of excitation — vortices and crowdions — all four forces emerge within a unified mechanical framework. Every proton and neutron is a vortex that creates a pressure drop propagating through the crystal as a 1/r field — this is gravity. The hyphons carry enormous base energy, but because it is perfectly uniform, only the excitations above it are visible as mass (Section 4). Light is a transverse wave propagating through the lattice; its speed depends on local lattice pressure, which is why clocks slow and light bends near massive objects (Section 3). Charge is the strain pattern a crowdion imposes on the surrounding lattice: same-type distortions repel, opposite types attract (Section 7). The strong nuclear force is surface contact energy between nucleon spheres packed in rock salt ordering, with electrons delocalizing between proton cores — the same mechanism as chemical bonding, operating at nuclear distances (Section 6). The weak nuclear force is the energy threshold for the electron to escape the neutron's surface orbit; beta decay is this escape (Section 5.5).

 doi:10.20944/preprints202604.0421.v1

The model produces quantitative predictions. The electron mass, proton mass, and fine structure constant are connected through the Frenkel-Kontorova kink mass formula for crowdions in FCC lattices. The coupling constant g is constrained close to unity by the twelve-fold FCC coordination geometry. From g, the fine structure constant is computed from the crystal's geometry and coupling parameters as $1/\alpha = 152$ (measured: 137). A single calibration — g from 0.81 to 0.998 — closes the gap, and the required value corresponds to a Morse potential steepness between silver and lead in the experimental tabulation of FCC metals (Section 9). The neutron's charge distribution — positive core, negative shell — is reproduced as the difference between two screening patterns, with one fitted parameter matching the data to 1% (Section 5.3).

Section 2 describes the structure of space and derives the hyphon size. Section 3 treats light as a lattice wave. Section 4 develops gravity as a pressure gradient. Section 5 describes particle structure: electron, proton, neutron, and their form factors. Section 6 covers nuclear structure and electron delocalization. Section 7 addresses charge and magnetism. Section 8 extends the picture to chemistry. Section 9 presents the quantitative predictions.

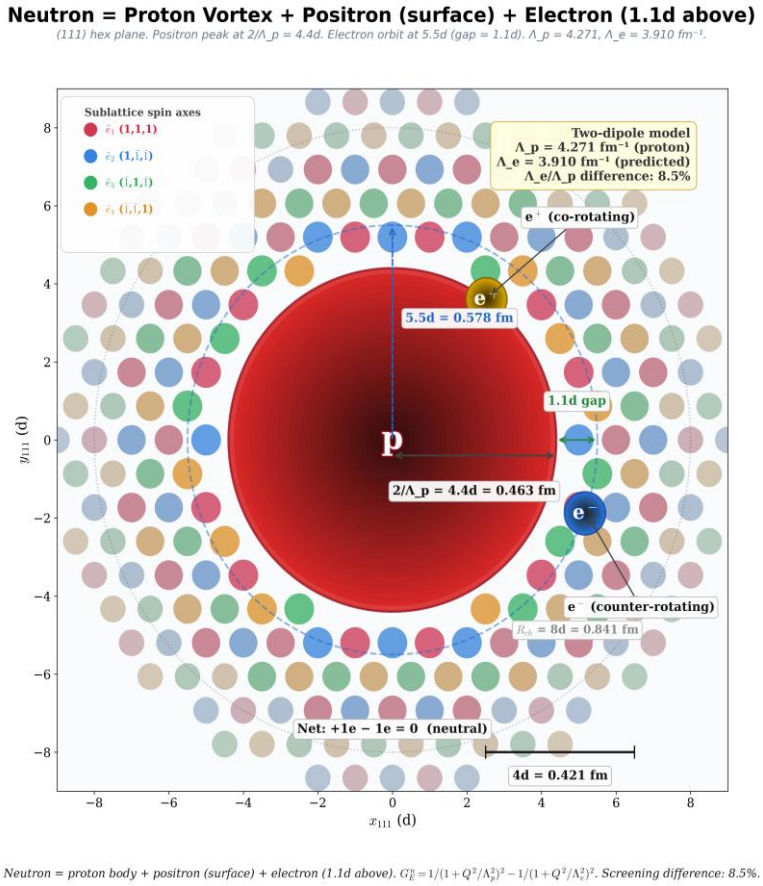

Figure 1. The neutron as a proton vortex with positron (surface) and electron (1.1d above). Cross-section along the hexagonal plane showing the proton body (red, equivalent sphere radius 4.4d = 0.46 fm, approximately 1000 hyphons) with positron crowdion (gold, on surface) and electron crowdion (blue, orbit at 5.5d from centre). Charge radius R_ch = 8d = 0.84 fm (dotted). The surrounding FCC hyphon lattice is colour-coded by sublattice spin axis. Net charge: +1e − 1e = 0 (neutral).

2. Foundation: Structure of Space

2.1. The Ether Lattice

In the proposed model, all physical reality is composed of a single substance: a superfluid ether. The fundamental particle of this framework is the hedron (from Greek hedra, ἕδρα, meaning

 doi:10.20944/preprints202604.0421.v1

foundation; symbol η), the base unit of ether whose size has not been determined. Hedrons organise into hyphons (from Greek hyphē, ὑφή, meaning fabric; symbol υ)—near-spherical structures of outer diameter d = 0.105 fm, each spinning on a single axis. These hyphons form the fabric of space, arranged in a face-centred cubic (FCC) lattice—the same crystal structure as copper or aluminium, and the densest possible packing of equal spheres. The FCC unit cell contains four elements, each belonging to a different sublattice. The four sublattice spin axes point along the four directions of a regular tetrahedron: (1,1,1), (1,−1,−1), (−1,1,−1), and (−1,−1,1), normalised. A spinning element resists impulses perpendicular to its spin axis (flywheel effect) but not along it. For any direction of impulse, the total flywheel resistance from the four sublattices sums to exactly 8/3—a constant, independent of direction. This is a mathematical identity of the regular tetrahedron (a spherical 2-design) and guarantees that the speed of light is isotropic without fine-tuning. The hyphon size corresponds to the healing length of the superfluid—the characteristic scale at which the medium recovers from a disturbance, directly analogous to the healing length in superfluid helium-4.

Each hyphon has twelve nearest neighbours arranged in a cuboctahedron—the coordination geometry of FCC. Adjacent elements belong to different sublattices and spin on axes 109.5° apart. Hedrons also fill the gaps between neighbouring hyphons in the close-packed lattice, mediating the mechanical coupling between hyphons whose spin axes differ. What we observe as a neutrino is one or more hedrons ejected at high kinetic energy during a particle transition — the energy is set by the decay that produced them, which is why neutrinos appear at different energies without being fundamentally different particles. The hyphon size is set by lattice pressure: higher pressure compresses the hyphons into smaller, stiffer vortices, raising the speed of light; lower pressure allows them to expand and soften, lowering it. This is the same physics observed in superfluid helium-4, where the quantised vortex core diameter shrinks under pressure and expands at low pressure — at sufficiently negative pressure (−6.9 bar) the core expands without limit and the vortex ceases to exist (Maris, 1994). Far from mass, lattice pressure is high, the hyphons are maximally compressed, and the speed of light approaches an asymptotic ceiling. Near mass, the pressure drops, hyphons expand, and the local speed of light decreases. The same bridging mechanism operates at larger scales — nuclear binding (Section 6.1) is mediated by the approximately 1.6d of hyphon lattice between nucleon screening surfaces in rock salt ordering.

The closest laboratory analogue to the hyphon lattice is the quantised vortex lattice in rotating superfluid helium-4 (Yarmchuk, Gordon & Packard, 1979): identical vortex elements arranged in a regular triangular grid, each with fixed quantised circulation and fixed core size. Viewed along a body diagonal, the hyphon FCC lattice has the same triangular cross-section. In both systems, the medium itself (helium-4 atoms or hedrons) is something deeper — the vortices are organised structures within that medium. The individual vortex tubes in the He-4 grid are the analogue of hyphons — the lattice elements. Larger vortex rings that move through this lattice correspond to particles moving through the hyphon lattice. The critical rotation rate Ω_{c2}, at which vortex cores overlap and the lattice melts into continuous fluid, corresponds to particle formation — the proton's interior is fused continuous fluid where the FCC lattice has been destroyed. A black hole is the same process at extreme scale. The estimated He-4 vortex core rotation speed is approximately 0.7 times the speed of sound in helium — individual vortices spin below the wave speed, yet the lattice collectively transmits sound at the full wave speed. This grounds the assumption that hyphons spinning below c collectively transmit light at exactly c.

The hyphons carry energy—every vortex is a circulating structure, and circulation is kinetic energy. The undisturbed lattice therefore has an enormous energy density. However, this energy is perfectly uniform throughout free space. Because gravity in this model arises from lattice pressure gradients (see Section 4), not from absolute energy density, a uniform background produces no gravitational effect and no observable mass.

Two mechanisms break down the lattice: at galaxy edges, where insufficient energy density can no longer sustain the lattice structure and it reverts to unstructured ether; and inside black holes, where the extreme concentration of vortex energy overwhelms the lattice (see Section 2.4). Beyond

Preprints.org (www.preprints.org) | NOT PEER-REVIEWED | Posted: 7 April 2026 doi:10.20944/preprints202604.0421.v1

the observable universe, the hedron fluid has not yet accumulated enough energy to crystallise into a lattice (see Section 2.5).

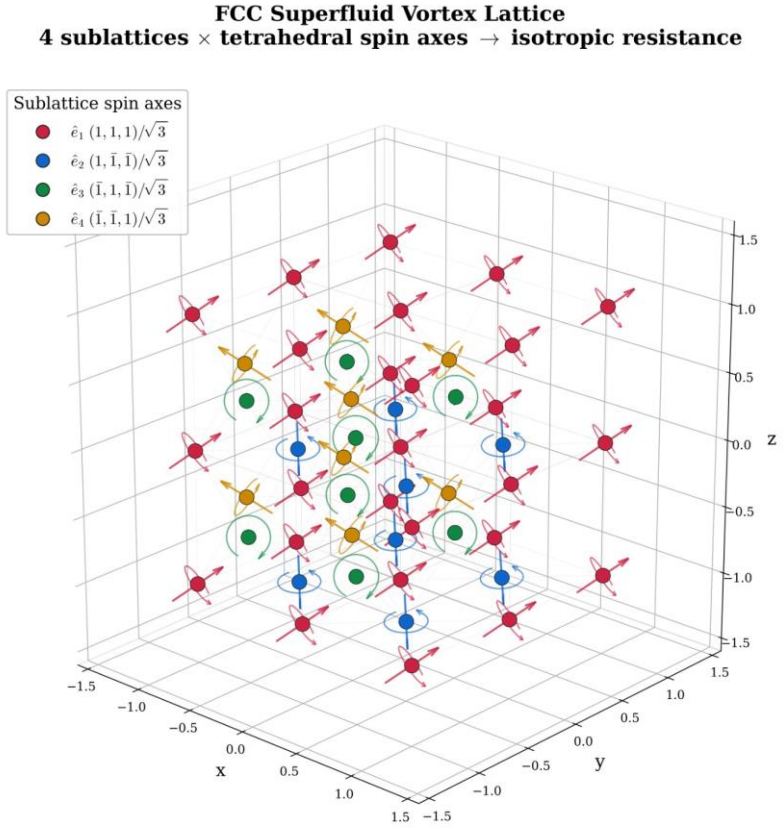

Figure 2. The FCC superfluid vortex lattice. Each hyphon (sphere) spins on its local tetrahedral axis, colour-coded by sublattice: $\hat{e}_1$ (red, (1,1,1)/√3), $\hat{e}_2$ (blue, (1,−1,−1)/√3), $\hat{e}_3$ (green, (−1,1,−1)/√3), $\hat{e}_4$ (gold, (−1,−1,1)/√3). Arrows indicate spin axis orientation. The tetrahedral symmetry guarantees $\Sigma \sin^2\theta_i = 8/3$ for all impulse directions—perfectly isotropic flywheel resistance.

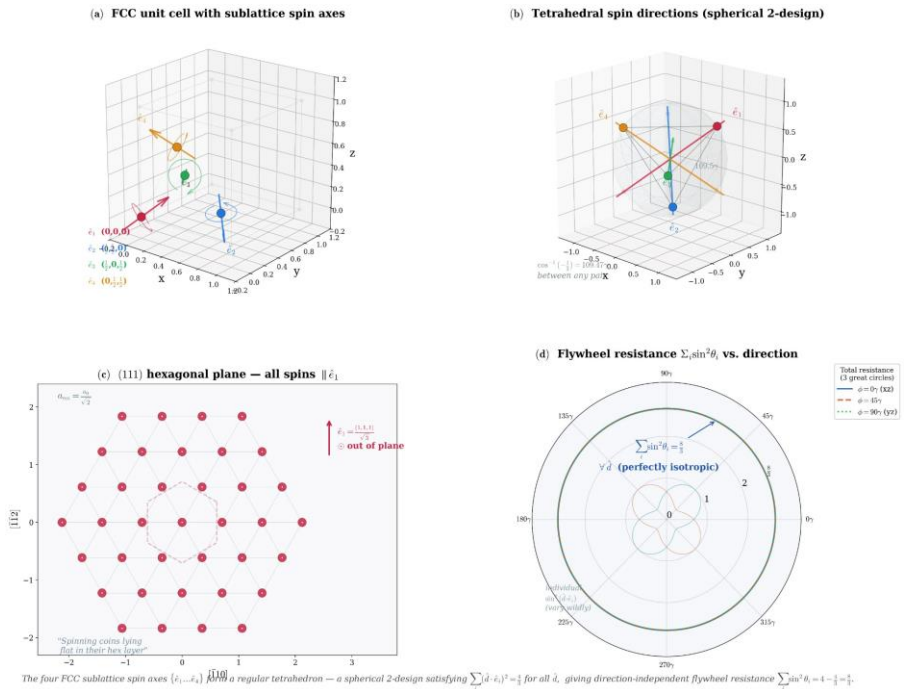

 doi:10.20944/preprints202604.0421.v1

Figure 3. FCC lattice geometry in detail. (a) The FCC unit cell with four subhyphons and their spin axes. (b) The four tetrahedral spin directions, separated by 109.5°, forming a spherical 2-design. (c) A (111) hexagonal plane—all elements in this layer belong to the same sublattice and spin parallel, like coins lying flat. (d) Polar plot of total flywheel resistance versus impulse direction: the sum $\Sigma \sin^2\theta_i = 8/3$ is constant for all directions (green circle), even though each sublattice's individual contribution varies wildly.

2.2. Energy States of the Ether

The ether exists in four states, distinguished by how much structure — and therefore energy — is present. Each transition toward greater order requires energy; destroying structure releases it.

At the lowest energy, the ether is an unstructured hedron fluid — disordered, with no lattice, no light, no matter. When sufficient energy is available, hedrons crystallise into hyphons — spinning spheres arranged in the FCC lattice. This crystallisation stores binding energy in the aligned structure: the ordered state is a higher-energy configuration, maintained by the spin coupling between neighbours. The spin creates the flywheel coupling that transmits impulses at c.

Within the lattice, further structure is possible. A proton is approximately 1000 hyphons organised into a coherent vortex — an excitation above the lattice ground state whose energy IS the proton mass (938 MeV). Destroying a proton releases this energy back into the lattice, as demonstrated by π^0 decay where 100% of the mass radiates as photons. The electron is a different kind of excitation — a crowdion soliton propagating through the lattice (see Section 5.1).

At the extreme, a black hole forms: the most energetic vortex structure, whose concentrated energy overwhelms the lattice entirely (see Section 2.4).

Each transition is reversible: add energy and structure builds upward; let energy radiate away and structure dissolves downward.

2.3. The Hyphon

The hyphon diameter is derived from the proton mass and lattice wave mechanics. In any crystal lattice with spacing a, the shortest possible wavelength is $\lambda = 2a$ — the Brillouin zone boundary, where adjacent atoms oscillate in opposite directions. The proton's reduced Compton wavelength $\hbar/(m_p c) = 0.2103$ fm is such a lattice wavelength, giving $d = \hbar/(2m_p c) = 0.1052$ fm.

Every hyphon carries rotational energy from its spinning structure. This energy is completely invisible — it is the uniform background against which all measurements are made. What we observe as "mass" is the excitation energy of vortex structures above this background — the circulation energy of the pattern, not the hyphons themselves.

The hyphon mass follows from the Frenkel-Kontorova kink mass formula $m_e/m_h = 2/(\pi^2\sqrt{g})$, where $g \approx 1$ for FCC lattices (Sections 5.1.2 and 9). This gives $m_h = m_e \times \pi^2/2 = 0.511 \times 4.935 = 2.522$ MeV. The mass ratio $N = m_p/m_h = 938.3/2.522 = 372$ gives the proton mass in units of hyphon masses — the excitation energy of the proton vortex above the lattice ground state.

This resolves the vacuum energy problem. Quantum field theory predicts vacuum energy 10^{120} times larger than observed because it assumes all vacuum energy gravitates. In this model, only pressure gradients produce gravity. The enormous uniform background energy creates no gradient and no gravitational effect. The cosmological constant measures residual non-uniformity at cosmic scales, not the total energy.

2.4. Black Holes

2.4.1. Structure and the Event Horizon

A black hole is a giant vortex in the superfluid ether — the same structure as a proton, scaled up until the concentrated energy overwhelms the lattice. The Schwarzschild radius $r_s = 2GM/c^2$ marks the shell where the hyphons expand beyond their stability limit and cease to exist as vortices — directly analogous to superfluid He-4 vortex cores at negative pressure, which expand without limit

 doi:10.20944/preprints202604.0421.v1

at −6.9 bar (Maris, 1994). A black hole is black not because light is too slow to escape, but because there is no lattice left to carry it.

Inside the event horizon lies unstructured ether — carrying the full rotational energy of everything that fell in, but with no structure to propagate it outward or concentrate it inward. General relativity predicts a singularity; the ether model has a pressure floor at zero. The energy disperses into the unstructured interior. What general relativity describes as a singularity is simply the boundary where the lattice ceases to exist.

2.4.2. Radiation and Evaporation

A black hole radiates because the boundary between structured lattice and unstructured interior is not static — it is a contact surface where the rotational energy of the interior meets the lattice ground state. The energy mismatch drives continuous energy transfer outward into the lattice. No quantum mechanics is required — no virtual particle pairs, no tunnelling — only the mechanical coupling between unstructured ether and the lattice at their shared boundary. Smaller black holes have tighter curvature, steeper energy gradients, and radiate faster — matching the standard prediction that radiation scales inversely with mass.

When mass falls into a black hole, more lattice is overwhelmed and the event horizon creeps outward — the infalling energy adds to the vortex concentration. Without infalling matter to sustain it, the black hole slowly radiates its stored energy outward: the event horizon contracts, and eventually the energy drops below the threshold at which particles can re-form. The cascade reverses: the radiated energy reconstitutes lattice → particles. The black hole evaporates into ordinary matter.

2.4.3. Black Hole Collisions and the Origin of Matter

The predominance of matter over antimatter may have a geometric origin. When two black hole vortices collide non-axially, the impact can eject vortex rings whose chirality is set by the collision geometry relative to the ABC stacking of the lattice. If such a vortex is below the black hole energy threshold, the lattice reforms around it and the vortex fragments into progressively smaller vortices, each inheriting the parent's chirality, until reaching proton size — the only stable toroid. Because chirality is preserved through the cascade, each such event produces a local excess of matter or antimatter. Whether this mechanism can account for the observed asymmetry has not been calculated.

2.5. The Observable Universe

In superfluid helium-4, the vortex state exists only within a specific pressure and temperature window. The ether lattice has analogous bounds. Lattice formation requires sufficient energy density — the hedron fluid must accumulate enough energy for spin alignment to crystallise. The observable universe is the region that has crystallised so far. Beyond its boundary lies the unstructured hedron fluid — not empty but featureless, carrying less energy per volume than the structured space we inhabit. No light propagates there because no lattice means no transverse waves — directly analogous to molten aluminium, which carries no transverse sound while the solid FCC crystal carries it at 3100 m/s.

At galaxy edges, far from the cumulative pressure contributions of surrounding matter, the lattice may thin toward its stability limit — the healing length grows, hyphons stretch apart, and the mechanical properties change. The anomalous flattening of galaxy rotation curves — conventionally attributed to dark matter — may instead reflect this lattice thinning: as the lattice stretches, the gravitational coupling deviates from the simple $1/r^2$ prediction derived for a uniform lattice. Where the lattice fails entirely, the ether reverts to its unstructured state — directly analogous to superfluid helium-4 below the critical rotation rate $\Omega c1$, where no vortices form and the fluid remains featureless.

 doi:10.20944/preprints202604.0421.v1

3. Light as a Lattice Wave

Light is a propagating wave in the ether lattice. It is not a particle. It is a transverse wave propagating through the lattice at the speed of light. Its energy is determined by its frequency—from radio waves to gamma rays.

This identification is not an analogy. In solid state physics, quantised lattice vibrations are called phonons. Their energy is $E = \hbar\omega$, they obey Bose-Einstein statistics, and their propagation speed is the speed of sound in the medium—a material property. Photons obey the same energy relation ($E = \hbar\omega$), the same statistics, and propagate at c—the speed of sound in the ether lattice. The quantum field theory formalism (creation and annihilation operators, Fock space) is identical for both. Phonons are quantised because the crystal is made of discrete atoms; photons are quantised because the ether lattice is made of discrete elements. The speed of light $c = 1/\sqrt{(\varepsilon_0\mu_0)}$ has the same mathematical structure as the speed of sound $v = \sqrt{(K/\varrho)}$, with the permittivity ε_0 playing the role of lattice compliance and the permeability μ_0 playing the role of inertial density. The electric and magnetic force constants were established independently—from electrostatic and magnetostatic experiments respectively—before Maxwell (1865) showed that their combination gives the speed of light. Three independent experiments, three separate phenomena, one number. If the ether lattice is discrete, a Debye-like cutoff should exist: a maximum photon frequency at which the wavelength equals twice the lattice spacing, above which electromagnetic waves cannot propagate.

3.1. Why Light Has No Longitudinal Mode

In FCC crystals, both longitudinal and transverse waves propagate — aluminium carries longitudinal sound at 6320 m/s and transverse at 3100 m/s. In the hyphon lattice, the transverse wave is light, travelling at c. The Cauchy relation for central-force FCC gives $K_{bulk} = 5G/3$, and the longitudinal speed follows:

$$v_l = \sqrt{((K_{bulk} + 4G/3)/\varrho)} = \sqrt{(3G/\varrho)} = c\sqrt{3} \approx 1.73c$$

Because the longitudinal speed exceeds c, all longitudinal energy is converted to transverse waves within a few lattice spacings, probably at a 1/3 decay rate per step. The bulk modulus is not infinite — what prevents longitudinal propagation is not incompressibility but the speed of light. This longitudinal-to-transverse conversion is routinely observed in ultrasonics: when a longitudinal wave in one metal exceeds the critical angle at an interface with a slower metal, it converts entirely to transverse waves — a standard technique in non-destructive testing. In the hyphon lattice, the longitudinal mode exceeds the speed limit everywhere, not just at an interface, so the conversion is immediate and complete. QED predicts photon energies to 13 decimal places, confirming that no energy leaks into an unobserved longitudinal channel.

3.2. Emission and Absorption

When a lattice impulse (light wave) reaches an electron, it transfers energy to the electron. The electron, being a crowdion soliton strongly coupled to the lattice, absorbs energy from the impulse. This energy changes the electron's speed and orbit. The reverse process—an electron dropping to a lower energy state—releases energy back into the lattice as an impulse that propagates away as a wave at the speed of light.

Atomic energy levels are quantised because the crowdion has discrete stable speeds set by the lattice periodicity (Section 5.1.4). Only specific speeds satisfy the Peierls-Nabarro barrier — the same physics that quantises crowdion velocities in FCC metals.

Light appears quantised at detection because the electron is a discrete object that absorbs energy in steps. Between emission and detection, the disturbance propagates as a continuous wave. No particle traverses space. The "photon" is a bookkeeping label for one quantum of energy transferred between an emitter and a detector via a lattice wave.

 doi:10.20944/preprints202604.0421.v1

The speed of light depends on the local lattice pressure—higher pressure yields faster propagation. This has directly measurable consequences (see Section 4.2).

3.3. Bell's Inequality and Lattice Waves

Bell (1964) proved that no theory in which particles carry predetermined values can produce correlations exceeding a certain bound. The CHSH formulation (Clauser et al., 1969) sets this bound at 2. Quantum experiments yield scores up to $2\sqrt{2} \approx 2.83$, violating this bound. This result has been widely interpreted as proof that nature is non-local—that measurement of one particle instantaneously affects a distant partner.

In the present model, light is not a particle carrying predetermined values—it is an impulse propagating through a continuous lattice. Two photons emitted from a common source (such as electron–positron annihilation) are correlated lattice waves sharing a common origin. Their phases, polarisations, and angular momenta are established at the moment of creation and carried independently through the lattice. Conservation laws guarantee that measuring one wave's properties constrains the other's—no signal needs to travel between them.

Whether correlated lattice waves in the FCC structure can quantitatively reproduce the $2\sqrt{2}$ violation of the CHSH bound has not been demonstrated. Bell's theorem was derived for point particles with hidden variables, not for extended waves in a discrete medium, and it is not obvious that its assumptions map onto the lattice model. A rigorous derivation of CHSH correlations from FCC lattice wave mechanics is an open problem. Until it is completed, the model's compatibility with Bell test results remains unresolved.

3.4. Light in Matter and the Michelson–Morley Experiment

In matter, light interacts with electrons in the atoms. Each interaction adds delay: more electrons per unit volume means a lower effective speed. This is refraction. The progression is continuous — from vacuum (no electrons, speed c) through glass and water to metals, where the electron density is so high that light cannot propagate.

The Michelson–Morley experiment (1887) found no variation in the speed of light with direction. In this model, the explanation is fundamental: particles are patterns in the hyphon lattice, not objects moving through it. A pattern moving through the lattice physically contracts in the direction of motion and its internal processes physically slow down — Lorentz contraction and time dilation are real mechanical effects, not coordinate artefacts. These effects exactly cancel any attempt to measure the pattern's motion through the lattice. This is what Lorentz proposed in 1892. Einstein's special relativity (1905) gives identical predictions. In this model, Lorentz invariance is not postulated — it emerges automatically because every measuring instrument is itself a pattern in the same medium it is trying to measure.

3.5. Open Question: Static Lattice or Ether Drag?

An alternative explanation exists for the Fizeau result and the Michelson–Morley null. If particle vortices physically drag the surrounding ether lattice — analogous to the mutual friction observed in laboratory superfluids (Hall & Vinen, 1956) — then matter would pull the lattice along with it, with a drag strength proportional to the electron density. In this picture, solid enclosures fully drag the local ether, explaining the Michelson–Morley null in enclosed experiments, while unshielded experiments might detect a residual wind. Miller (1925–1933) ran his interferometer on Mount Wilson in open air and reported a signal of approximately 9 km/s — disputed as thermal drift but qualitatively consistent with partial atmospheric drag. Both hypotheses — static lattice with emergent Lorentz invariance, and ether drag — produce the same Fresnel formula and the same null result in enclosed experiments. They differ in one prediction: the drag model predicts that an unshielded interferometer in space would detect the ether wind; the static-lattice model predicts it would not. Flyby anomalies — unexpected velocity changes observed during planetary gravity assists — may

 doi:10.20944/preprints202604.0421.v1

provide another test. In the static-lattice model, the anomalous velocities are measurement artefacts arising from lattice pressure variations around planetary bodies that alter the local speed of light. In the drag model, they arise from ether flow. Data from multiple flyby anomalies at different planets and distances could map the profile and distinguish pressure gradients from flow patterns. This question is not yet resolved.

4. Gravity

Every particle vortex — whether a single-hyphon electron soliton or a ~1000-hyphon proton — sustains internal circulation. A spinning vortex is inherently a low-pressure structure: the faster the internal flow, the lower the pressure at its core. The surrounding lattice, at higher pressure, pushes inward toward the low-pressure region. This inward push is spherically symmetric and decays as $1/r$ with distance. The resulting pressure gradient is gravity. The lattice itself is static — there is no bulk flow. Because every vortex creates a pressure drop, mass is always positive and gravity is always attractive.

The gravitational force between two masses follows the standard expression:

$$F = GMm / r^2$$

where G is the gravitational constant, encoding how much lattice stretch a vortex produces per unit of inertial mass. Nearly all measured mass comes from proton-scale vortices, so G is dominated by the proton's pressure drop. Whether the electron's much smaller contribution follows the same ratio has not been tested independently.

The perturbation is extraordinarily small. The dimensionless gravitational potential at Earth's surface is $GM/(Rc^2) \approx 7 \times 10^{-10}$ — roughly one part per billion. This is the fractional lattice stretch: each lattice spacing near the surface is longer by that fraction than a spacing far from any mass. Integrated over 100 km of altitude, the cumulative physical stretch totals approximately 70 micrometres — the width of a human hair spread across a distance one would drive in an hour. At the lattice scale, this amounts to one extra element spacing per 300 nanometres of radial distance. Gravity is detectable only because protons come in very large numbers: the Earth contains 3.6×10^{51} nucleons, each contributing its individual pressure deficit to the collective field.

4.1. Correspondence with General Relativity

General relativity is not incorrect—it is a mathematically precise description of wave propagation in a medium with position-dependent speed. Einstein identified the correct mathematical structure. The ether model provides the physical substrate that the mathematics describes.

The historical logic is as follows. Michelson & Morley (1887) failed to detect ether wind — in this model, because patterns in the lattice physically contract and time-dilate, making the medium fundamentally undetectable from within (see Section 3.4). Einstein concluded that no medium exists and that c is constant by postulate. But c observably varies near mass: clocks slow, light is delayed, and frequencies shift. Since c "cannot" vary by postulate, the variation was absorbed into the geometry of spacetime. Spacetime curvature is the pressure field, expressed in a formalism that obscures the medium.

The Shapiro delay is consistent with this picture. Radar signals sent past the Sun to a planet and back take measurably longer when the path passes close to the Sun—approximately 200 microseconds of excess delay for a signal grazing the solar limb. In the ether model, the signal passes through a region of stretched lattice near the Sun, where both the reduced density and the stretching itself may contribute to the delay.

The speed of light is the transverse wave speed of the lattice — the same kind of wave as transverse sound in an FCC metal. Near mass, the lattice pressure drops and the hyphons expand: larger, softer vortices transmit impulses more slowly, just as superfluid He-4 vortex cores expand

 doi:10.20944/preprints202604.0421.v1

and soften at lower pressure. The local speed of light drops. This does not mean that the particles themselves slow down. A proton vortex near a massive body still carries the same internal circulation. What changes is the medium around it — the hyphons that carry light, transmit forces, and define the local clock rate. Clocks slow near mass because their mechanism depends on lattice wave propagation, which is slower when the hyphons are softer.

There is a maximum lattice pressure with a corresponding maximum speed of light, set by the maximum stiffness of the compressed hyphons (see Section 2.1). Starting from a black hole at zero pressure, the speed of light increases with distance from any mass but approaches an asymptotic ceiling it never exceeds.

4.2. Possible Deviations from 1/r

The $1/r$ pressure decay (yielding $1/r^2$ force) is an excellent approximation in the regime of precise measurement. It is known to fail inside the proton core, where the vortex structure has its own internal pressure profile. The $1/r$ approximation becomes valid only outside the core. Whether $1/r$ holds exactly at all distances remains an open question.

The Kuiper cliff: the Kuiper Belt density drops sharply at approximately 50 AU. The hypothesised Planet Nine (5–10 Earth masses at 400–800 AU, unfound after a decade of searching) may be unnecessary. If $1/r$ becomes nonlinear at large distances, the Sun's gravitational field would weaken faster than expected, producing a sharper edge than the $1/r^2$ prediction.

4.3. Gravitational Waves

Gravitational waves are transverse waves propagating through the ether lattice at the speed of light, as detected by LIGO (Abbott et al., 2016). Both light and gravitational waves are transverse and travel at c, but they differ in polarisation geometry: light (spin 1) has two polarisation states separated by 90°, while gravitational waves (spin 2) have two states separated by 45°. In the FCC lattice, this distinction maps to direction families: spin 1 corresponds to the [100]↔[110] angle (45.00°) and spin 2 to the [110]↔[111] angle (35.26°). The same lattice geometry that produces spin-1/2 particles at [100]↔[111] (54.74°) naturally accommodates both electromagnetic and gravitational waves as distinct transverse modes.

5. Particle Structure

The macroscopic analogue of a vortex particle is a bubble ring — a toroidal air bubble stabilised by poloidal circulation of the surrounding water. Air bubbles smaller than approximately two centimetres remain spherical; larger bubbles transition to toroidal form as the internal pressure differential punches through the centre (Bonometti & Magnaudet, 2006). This sphere-to-toroid transition is the bubble analogue of the mass gap between monopole and dipole particles: below a critical size, surface tension holds the vortex spherical; above it, the circulation opens an eye. Bubble rings in water also offer the best available visualisation of particle decay: they form, rearrange, split into smaller rings, and transform between toroidal and spherical shapes — not a perfect analogy, but the easiest way to see how vortex structures break apart.

5.1. The Electron

The electron is identified as a crowdion soliton — a propagating interstitial defect in the hyphon FCC lattice. The crowdion is a well-studied object in condensed matter physics with experimentally confirmed properties that correspond one-to-one to the known properties of the electron.

5.1.1. The Crowdion

In condensed matter physics, a crowdion is an extra atom forced into a close-packed row of a crystal. The extra atom displaces its neighbour, which displaces the next, and the disturbance propagates as a soliton while the lattice heals behind it. No single atom travels the full distance — the

 doi:10.20944/preprints202604.0421.v1

"particle" is the pattern, not a physical object. Crowdion propagation has been confirmed by molecular dynamics simulations in FCC metals including aluminium, nickel, and lead, with speeds up to 11 km/s (Shepelev et al., 2023).

5.1.2. Crowdion–Electron Correspondence

Every property of the crowdion listed below has been measured or simulated in real FCC metal crystals. The right column shows the corresponding electron property.

Crowdion (measured in FCC metals)	**Electron**
Speed is lattice-determined, not launch-determined. Only specific speeds are stable.	Quantised energy levels.
Carries one atom's worth of displacement. Effective mass from lattice potential (FK kink mass).	Rest mass from lattice geometry ($m_e = m_h \times 2/(\pi^2\sqrt{g})$).
Carries topological charge — a point carrier of deformation.	Electric charge — a point carrier of lattice distortion.
Parallel crowdions repel via lattice strain.	Like charges repel via Coulomb interaction.
Radiates phonons when decelerating near a defect.	Radiates photons when decelerating (bremsstrahlung).
Obeys relativistic dispersion $E = m^*c^2/\sqrt{(1 - v^2/c^2)}$.	Obeys special relativity.
FCC lattice has two mirror-image propagation handednesses.	Electron (−1e) and positron (+1e).

The crowdion physics is established. The mapping to electron physics is the proposal of this paper.

5.1.3. The Electron as Crowdion

The electron is a crowdion that moves through the FCC lattice as a soliton. A free electron is this impulse propagating in a straight line; a bound electron is the same impulse bent into a closed loop by a proton's pressure well. There is no stationary electron — only smaller orbits. The electron travels along [111] channels — the lowest-energy path through the lattice — tilted at 54.74° from the cube edges, the spin-1/2 angle. The positron is the same crowdion with opposite chirality. The electron is always charged because the crowdion disrupts the surrounding lattice at every position — charge is not something the electron carries but something the electron is: a permanent misfit. It is stable because there is no smaller lattice excitation to decay into.

The electron-as-soliton idea has a long history (Ekholdt, 2009), following de Broglie's original wave-particle programme. What appears to be new here is identifying the electron specifically as a crowdion — an interstitial defect soliton in a physical FCC lattice with known spacing (d = 0.105 fm) — and obtaining its mass from the Frenkel-Kontorova effective mass formula.

5.1.4. Electron Mass

The crowdion settles into a speed determined by the lattice, not by the initial kick. There is a velocity window: too slow and it is trapped by the Peierls-Nabarro barrier; too fast and it becomes unstable, radiating energy until it breaks apart. The crowdion energy follows the relativistic dispersion relation $E = m^*c^2/\sqrt{(1 - v^2/c^2)}$, where c is the speed of sound in the crystal. The Frenkel-Kontorova model gives the crowdion rest mass as $m_{kink}/m_{atom} = 2/(\pi^2\sqrt{g})$, where g is a dimensionless coupling constant set by the ratio of in-row spring stiffness to off-row barrier height

 doi:10.20944/preprints202604.0421.v1

(Braun & Kivshar, 1998). The 12-fold coordination of FCC constrains g close to unity (Section 9). Computing g from first principles — deriving the Morse steepness from FCC spin frustration, torsional stiffness, and the wave speed constraint v = c — gives α_Morse ≈ 3.8 and g ≈ 0.81, yielding $1/\alpha = 152$ (11% above measured). The remaining gap traces to known approximations in the stiffness calculation (Section 9). The measured fine structure constant requires g = 0.998, corresponding to α_Morse ≈ 4.4. This steepness lies between silver (4.26) and lead (4.42) in the experimental tabulation of FCC metals by Girifalco & Weizer (1959) — the hyphon lattice has the same dimensionless potential shape as an ordinary FCC metal. The calibration from g = 0.81 (computed) to g = 0.998 (required) is a 19% adjustment, comparable to the estimated uncertainty in the first-principles calculation. The charge mechanism and its consequences are discussed in detail in Section 7.

5.2. The Proton

The proton is approximately 1000 hyphons organised into a toroidal vortex with a positron (counter-rotating crowdion) orbiting on its surface. The most likely geometry is a toroid with tube radius a ≈ 2.3d, ring radius R ≈ 7.3d, and an open eye. The vortex is a self-sustaining circulation pattern: hyphons enter at the leading edge, circulate, and return to their ground state at the trailing edge. The pattern is permanent; the participants are temporary. This is proven by π^0 decay, where 100% of the 135 MeV mass radiates as photons — no hyphon leaves the lattice, only the circulation energy is released, confirming that the mass is entirely excitation energy above the ground state.

When a vortex splits or dissolves, hyphons that were part of the collective rotation must return to the ground state lattice. Inside the vortex, the 26% interstitial gap space participated in the circulation — the hyphons were packed differently than in the undisturbed lattice. Some hyphons have no room in the restored structure and are squeezed into close-packed rows as crowdion–anticrowdion pairs: electron–positron pairs. They appear as pairs because the total lattice displacement must balance. The counter-rotating crowdion is mechanically attracted to the nearest vortex surface and becomes the positron that provides confinement. The co-rotating crowdion is repelled and escapes as a free electron.

The proton's charge (+1e) is carried by a counter-rotating positron crowdion on the vortex surface. The antiproton is the same structure with an opposite-chirality crowdion. The measured charge radius (0.84 fm = 8.0d) reflects the orbit-averaged charge distribution, not the vortex boundary.

What determines whether a vortex is stable remains an open question. The eta prime meson (η', 958 MeV), a spin-0 particle heavier than the proton (938 MeV), decays in 10^{-21} s — suggesting that mass alone does not guarantee stability and that the internal topology of the vortex plays a decisive role. One possible mechanism is mechanical confinement by the surface crowdion: as the positron orbits the toroid both toroidally and poloidally, it may act as a wound wire compressing the vortex body inward. This would explain the lifetime progression from the neutral pion (π^0, no crowdion, 10^{-17} s) through the charged pion ($\pi\pm$, one loop, 10^{-8} s) to the proton (full surface coverage, stable). If the positron's orbit is what holds the proton together, then removing it — as may occur in deep inelastic scattering at high Q^2 — would allow the vortex to dissolve entirely into radiation, representing complete conversion of mass to energy without the need for antimatter.

The proton mass (938.3 MeV) is excitation energy — the energy cost of maintaining the vortex circulation above the lattice ground state. In FCC close packing — the cannonball stacking — spheres occupy 74% of the volume and the gaps between them occupy 26%. When hyphons organise into a coherent vortex, the interstitial fluid in these gaps joins the collective rotation. The ratio of gap volume to sphere volume (26%/74% ≈ 35%) sets the excitation fraction: the proton mass is approximately 35% of the total hyphon mass in the vortex. This gives N_vortex ≈ 938/(0.35 × 2.522) ≈ 1060 hyphons, consistent with the toroid geometry. The mass ratio N = m_p/m_h = 372 counts hyphon-masses' worth of excitation energy, not the number of physical hyphons in the vortex.

The proton's spin axis aligns with one of the four body diagonals of the FCC lattice, tilted at 54.74° from the cube edges — the same angle as the electron, because both are spin 1/2. This gives

 doi:10.20944/preprints202604.0421.v1

four possible orientations, each with two possible flow directions, yielding eight distinct proton/antiproton states.

The measured electric form factor is a dipole: $G_E = 1/(1+Q^2/\Lambda^2)^2$ with $\Lambda = 4.271$ fm^{-1}. The dipole shape arises because the positron crowdion orbits both toroidally and poloidally, but the time-averaged orbit produces a single effective charge radius $R_{eff} = \sqrt{(R^2 + a^2)}$ — two geometric scales produce a single effective charge radius at low Q^2. The correlation between spin, orbit topology, and form factor power is discussed in Section 5.4.

The dipole produces a real-space charge density $\varrho(r) \propto \exp(-\Lambda r)$, peaking at $r = 0$ with RMS charge radius $\sqrt{12}/\Lambda = 0.81$ fm. This does not mean the charge is at the centre — any source convolved with Yukawa[2] screening produces a centre-peaked exponential. The physical charge source is the crowdion orbit on the vortex surface. The measured charge radius at 8d reflects the orbit-averaged distribution, not the vortex boundary.

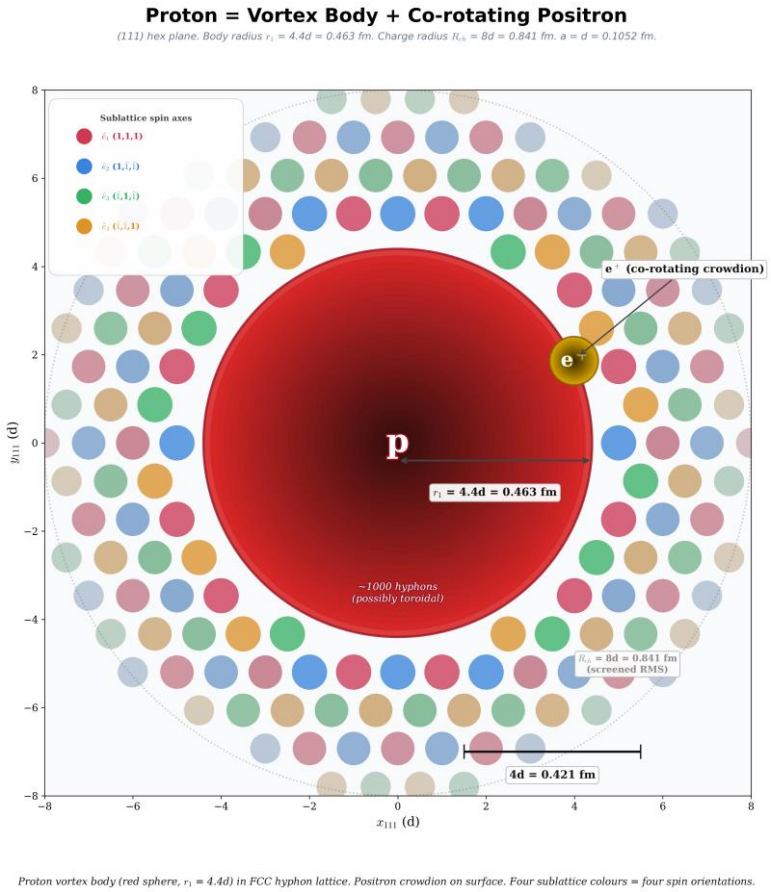

Figure 8. Proton vortex body (red, equivalent sphere radius 4.4d = 0.46 fm, approximately 1000 hyphons) in the FCC hyphon lattice hexagonal plane. Positron crowdion (gold) counter-rotates on the vortex surface. Dotted circle: charge radius R_{ch} = 8d = 0.84 fm (screened RMS). Four sublattice colours correspond to the four spin orientations. Lattice spacing a = d = 0.105 fm.

5.3. The Neutron

The neutron is the same toroidal vortex — same geometry, same ~1000 hyphons — with an electron orbiting at approximately 5.5d from the centre (1.1d above the vortex surface). The electron's opposite charge (−1e) cancels the proton's charge (+1e) when seen from outside, giving net charge zero. This is directly measured: the neutron's charge form factor shows a positive core and a negative exterior, and the measured squared charge radius $\langle r^2 \rangle_n = -0.1161$ fm^2 is negative because the electron sits outside the proton's vortex body. The neutron's mass (939.565 MeV) equals the proton mass

 doi:10.20944/preprints202604.0421.v1

(938.272 MeV) plus the electron mass (0.511 MeV) plus a binding energy of 0.782 MeV required to bind the electron in orbit.

Beta decay occurs when a lattice fluctuation gives the electron enough energy to escape the surface orbit. The proton's charge is fully exposed and positive charge reappears. The 880-second lifetime reflects how tightly the electron is bound. Inside a nucleus, neighbouring nucleons constrain the geometry further, which is why bound neutrons are stable.

The neutron's charge structure can be derived quantitatively. Both the proton and the electron are spin 1/2, so both produce dipole charge patterns through the lattice. The proton's pattern is measured directly: $G\_E^p = 1/(1+Q^2/\Lambda_p^2)^2$ with $\Lambda_p = 4.271$ fm^{-1}. The electron, as an orbiting crowdion soliton, also creates a dipole pattern with its own screening parameter Λ_e. The neutron's electric form factor is the difference: $G\_E^n = 1/(1+Q^2/\Lambda_p^2)^2 - 1/(1+Q^2/\Lambda_e^2)^2$.

The electron's screening parameter can be predicted from geometry. The lattice has an intrinsic screening rate Λ_0, the same for both particles. Each particle's effective screened charge radius adds its source radius in quadrature: $12/\Lambda\_eff^2 = R\_source^2 + 12/\Lambda_0^2$. Calibrating Λ_0 from the proton (R_p = 0.42 fm, $\Lambda_p = 4.271$ fm^{-1}) gives $\Lambda_0 = 4.996$ fm^{-1} — an intrinsic screening length of 0.20 fm ≈ 2d. The electron's effective source radius is $R_e \approx 0.55$ fm. Substituting gives $\Lambda_e = 3.914$ fm^{-1}. Fitting Λ_e directly to the measured Galster neutron form factor gives 3.877 fm^{-1} — agreement to 1%.

The two-dipole model reproduces the measured neutron charge distribution: a positive core (0 to ~0.73 fm) where the proton's tighter screening dominates, a negative shell (0.73 to ~2 fm) where the electron's wider screening dominates, and a mean square charge radius $\langle r^2 \rangle_n \approx -0.13$ fm² (measured: −0.116 fm², 8% off). The 9.2% difference in screening length between proton and electron — the single number that determines the neutron's entire charge structure — is a geometric consequence of their different source radii within the same lattice.

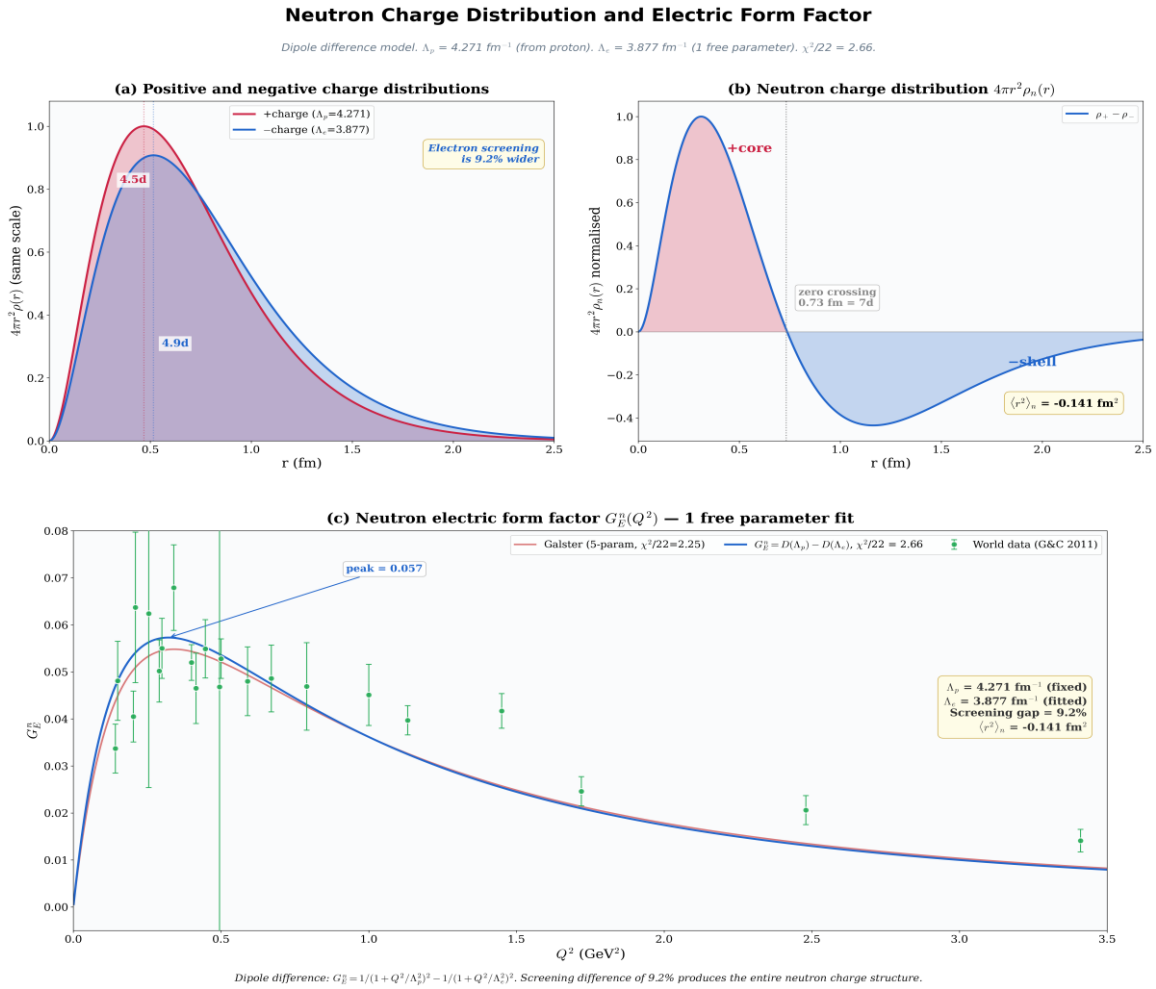

 doi:10.20944/preprints202604.0421.v1

Figure 9. Neutron charge structure. (a) Physical structure: proton vortex body (4d, red) with electron orbit (blue shading) and screening radii $R\_ch^p = 7.7d$, $R\_ch^e = 8.4d$. (b) Two nearly identical dipole distributions on the same scale: proton (Λ = 4.271 fm^{-1}) and electron (Λ = 3.877 fm^{-1}), differing by 9.2% in width. (c) Neutron charge distribution: model (blue) versus Galster measurement (red), showing positive core, zero crossing at 0.75 fm, and negative shell. (d) Neutron electric form factor G_E^n: model versus measured data across $Q^2 = 0$ to 2.5 GeV^2.

5.4. Spin, Form Factors, and Stability

In this model, spin describes whether and how the charge defect orbits within the vortex. The FCC lattice has exactly three angles between its principal direction families, and the quantum-mechanical tilt formula $\cos\theta = s/\sqrt{(s(s+1))}$ produces the same angles from half-integers:

Spin	FCC directions	Angle	Form factor	Particles	Stable?
0	—	—	Monopole ($1/Q^2$)	$\pi\pm$, K±	All unstable
1/2	[100] ↔ [111]	54.74°	Dipole ($1/Q^4$)	e, p, n, Σ^-	e, p stable
3/2	Not principal	39.23°	—	Ω^- (10^{-10} s)	All unstable
2	[110] ↔ [111]	35.26°	—	—	None observed

A correlation is observed between spin and form factor type. Spin-0 particles ($\pi\pm$, K±) all have monopole form factors — consistent with a crowdion orbiting on a sphere or closed-eye toroid, producing one geometric scale. Spin-1/2 particles (proton, neutron) have dipole form factors — consistent with a crowdion winding both toroidally and poloidally on an open-eye toroid, producing two geometric scales. The form factor column lists measurements, not fits — zero exceptions have been found.

The photon (spin 1) is not a vortex structure — it is a transverse lattice wave (Section 3). Its two polarisation states correspond to spin 1, but the orbit interpretation does not apply.

5.5. The Weak Nuclear Force and Symmetry Violations

The weak nuclear force does not exist as a separate force in this model. The neutron is a proton with an electron orbiting 1.1d above the vortex surface (Section 5.3). Beta decay occurs when the electron gains enough energy to escape this orbit. Electron capture is the reverse — an external electron falls into the same orbit. What standard physics attributes to the weak interaction is simply the energy threshold for entering or leaving a close orbit around a proton core.

The FCC lattice with ABC stacking is intrinsically chiral — ABCABC and CBACBA are mirror images that cannot be superimposed. Any process that depends on local lattice geometry automatically violates parity (P). Of the four forces, only the weak force sees this chirality. Gravity is a bulk pressure gradient with no stacking dependence. Electromagnetism propagates equally in all directions. The strong force operates through symmetric surface contact between nucleon vortices. But beta decay — electron entry into and exit from a specific lattice site — depends on the local site geometry, which is ABC-dependent. This is why parity violation is observed exclusively in weak interactions.

The standard model requires electroweak symmetry breaking and the Higgs mechanism to produce parity violation. In this model, P violation is mandatory from the geometry. Whether the same lattice chirality also accounts for C and CP violation requires further investigation.

5.6. The Lorentz Factor and Rotational Speed

The relativistic energy formula $E = \gamma mc^2$, where $\gamma = 1/\sqrt{(1 - v^2/c^2)}$, was derived by Hendrik Lorentz between 1892 and 1904 from the mechanics of objects moving through a stationary ether, before Einstein reinterpreted the same equations without reference to a medium.

 doi:10.20944/preprints202604.0421.v1

In the vortex model, γ describes the energy cost of pushing a vortex through the ether lattice at translational speed v. As a vortex approaches c, the hyphons ahead have less and less time to move aside—the displacement signal travels at c, barely ahead of the vortex. At v = c the signal cannot propagate ahead at all, an infinite column of hyphons must be displaced simultaneously, and the energy diverges.

This is strictly a translational phenomenon. A spinning vortex does not push a column of lattice ahead—it rotates in place. Its neighbours feel the mismatch, but there is no infinite-column problem. Rotational speed has no theoretical ceiling. A vortex can spin at any rate. It cannot do so stably—the lattice bleeds energy from the over-spun vortex—but the instability is energetic, not kinematic. There is no rotational equivalent of the γ divergence.

6. Nuclear Structure

Nucleons are identical spheres — approximately 1000 hyphons organised into vortices of diameter 8.0d. Protons carry charge (+1e); neutrons are the same sphere with a surface electron cancelling the charge. Inside nuclei, these spheres pack in rock salt (NaCl-type) ordering: protons and neutrons on alternating sublattices. The entire rock salt structure inherits the 54.74° tilt from the hyphon lattice — all nucleon spin axes point along body diagonals, and the natural packing planes are (111) hexagonal layers. The arrangement of nucleons on an FCC lattice with alternating proton-neutron ordering has a substantial history. The FCC symmetry of nuclear quantum states was first identified by Wigner (1937). Cook (1994, 2006) developed this into a comprehensive lattice model, showing that the FCC geometry reproduces the quantum numbers of the independent-particle model, the liquid drop properties, and alpha cluster substructures within a single framework — and computed binding energies for over a thousand nuclei and charge radii for 341 isotopes. Garai (2003) showed that the proton positions in FCC double tetrahedra correlate with all nuclear quantum numbers. The present work arrives at the same nuclear ordering from a different starting point: the rock salt alternation emerges from Coulomb energetics of charged and screened vortex spheres, and the nuclear lattice is embedded within a more fundamental hyphon FCC lattice with a physical 1.6d gap between nucleon screening surfaces.

6.1. Rock Salt Ordering and Nuclear Density

The alternating arrangement arises from Coulomb energetics. All nucleon cores are identical proton-core vortices carrying charge +1e. In an N = Z nucleus, Z delocalized electrons flow through the lattice channels between them (Section 6.2). At any instant, a core with an electron nearby appears electrically neutral — a neutron — while a bare core appears as a proton. This proton–neutron distinction is a snapshot of the electron positions, not a permanent property of the cores. In this snapshot picture, the lowest-energy arrangement places protons and neutrons on alternating sites: each proton has 6 neutron nearest neighbours and vice versa, the standard rock salt geometry.

This ordering also follows from the sublattice geometry of the hyphon lattice itself. In the FCC structure, nearest neighbours always belong to different spin sublattices, while second-nearest neighbours belong to the same sublattice. The four tetrahedral spin orientations pair naturally into two antiparallel groups — {S0,S1} vs {S2,S3} — whose net spins oppose at 180°. This two-group alternation on an FCC lattice is rock salt ordering, which Canuto & Chitre (1974) showed is the antiferromagnetic ground state. The rock salt structure is therefore not assumed — it is the lowest-energy configuration that the hyphon lattice geometry requires.

In heavy nuclei at saturation density (0.16 nucleons/fm^3), rock salt ordering gives a nearest-neighbour distance of 17.6d = 1.85 fm. With nucleon charge diameter 16.0d (0.84 fm radius), this leaves a gap of approximately 1.6d between screening surfaces. Nucleons do not directly contact each other. Each nucleon meshes only with the hyphon lattice at its own surface.

He-4 (4 proton cores + 2 delocalized electrons) is the minimal rock salt unit — a square with cores of one orientation pair on opposite corners. Being the lightest nucleus, He-4 is less dense than bulk nuclear matter, with a nearest-neighbour distance of approximately 19.5d = 2.05 fm. Its charge

 doi:10.20944/preprints202604.0421.v1

radius (1.676 fm) is within 0.5% of twice the proton charge radius (0.841 fm). The discrete square geometry gives R_ch = √(d²_nn/2 + R²_p) = 1.676 fm — a 99.9% match to experiment. A tetrahedral arrangement (as in Cook's FCC model without sublattice ordering) gives approximately 1.50 fm — inconsistent with the measured value. The charge radius formula R_ch = √(3/5 × (r₀(2Z)^{1/3})² + R²_p), applied across 285 isotopes (Z = 1–83), gives $R^2 = 0.988$ — comparable to Cook's empirical result ($R^2 = 0.979$), confirming uniform proton-core density in the N = Z core.

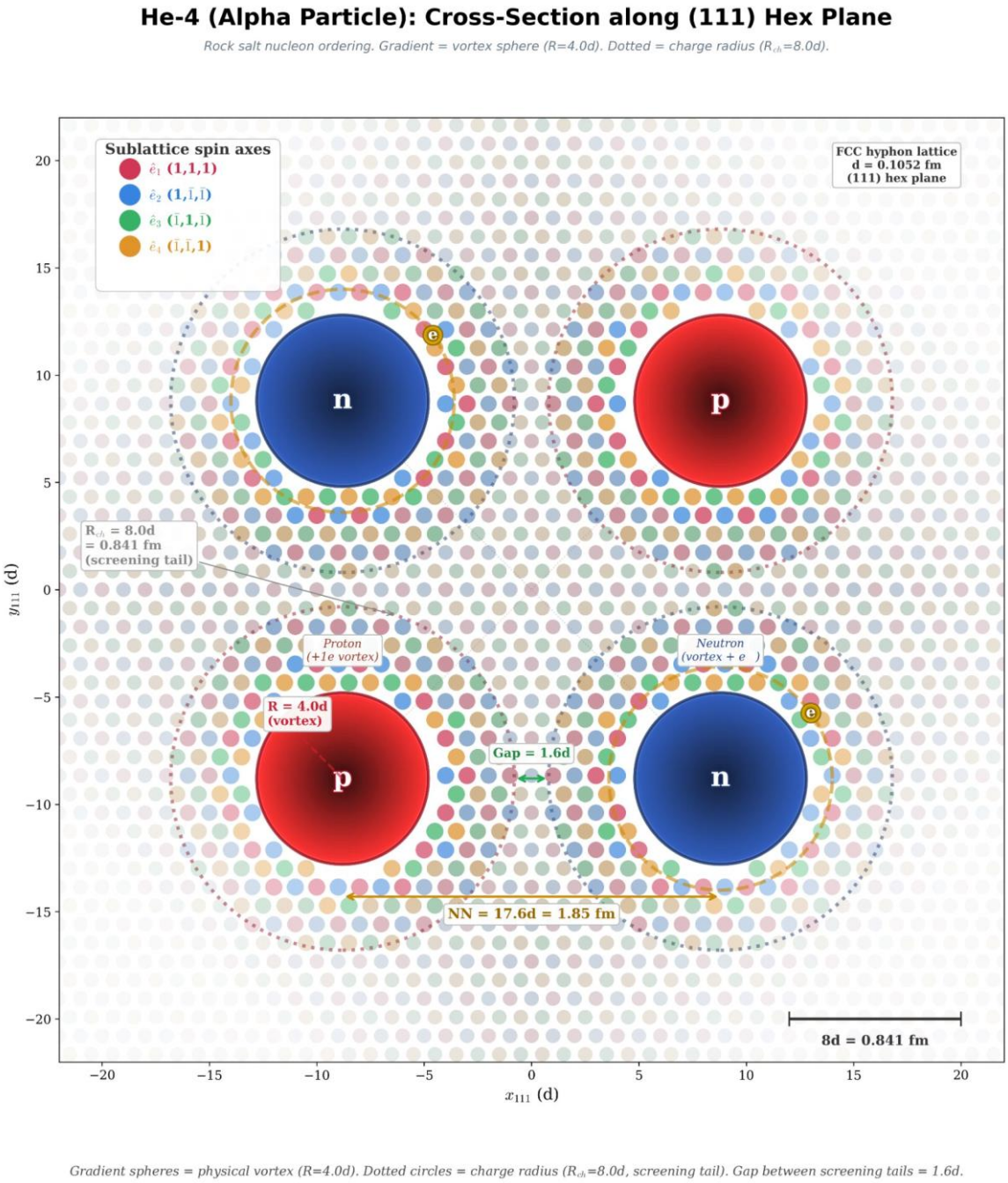

Figure 4. He-4 (alpha particle) cross-section along the hexagonal plane. Rock salt ordering places proton cores (red gradient, R = 4.0d) and neutron cores (blue gradient, vortex + electron) on alternating corners. Dotted circles show the charge screening tail (R_ch = 8.0d = 0.841 fm). Two delocalized electrons (yellow 'e') flow between cores. The FCC hyphon lattice (small colour-coded spheres, d = 0.1052 fm) fills all space outside the nucleon spheres. Centre-to-centre spacing 17.6d = 1.85 fm; gap between screening tails ≈ 1.6d. Three states of the same medium are visible: nucleon (fused vortex), electron (crowdion soliton), hyphon (spinning sphere, neutral).

 doi:10.20944/preprints202604.0421.v1

The rock salt picture is a bulk approximation that works well for nuclei above carbon ($A \geq 12$, charge radius errors below 3%) but breaks down for light nuclei — errors exceed 20% for $A \leq 4$, where a uniform-density sphere is meaningless for just a few nucleon cores. For these systems, the charge radii and binding energies depend on the specific geometry of proton core positions and the delocalized electron orbits described in the next section, requiring a detailed treatment of Coulomb screening and the strong force rather than a statistical bulk formula.

6.2. Electron Delocalization Inside Nuclei

In a free neutron, the electron orbits at approximately 5.5d from the proton centre with binding energy 0.782 MeV — barely bound, as demonstrated by the neutron's 10-minute decay half-life. When a second proton core approaches to nuclear distance, its Coulomb pull on the electron competes with the parent proton's hold. The electron, already on the verge of escape, detaches from one core and is captured by the other. The resulting orbit is a shared path between the two cores — most likely a figure-8 with the crossing point between them, though an elongated racetrack (two half-orbits connected by near-straight segments along the cores' edges) is also geometrically possible depending on the electron speed and core separation. In either topology, the electron visits both proton cores in each cycle, screening their mutual Coulomb repulsion. The idea that neutron electrons delocalize between proton cores inside nuclei was independently proposed by Cziráki (2023), who described the nucleus as protons held together by collectivized electrons in a covalent-like bond. The present work arrives at the same conclusion from a different starting point — the hyphon lattice mechanics — and develops the orbital geometry, screening calculations, and geometric frustration picture in detail.

Once detached, the electron flies to the neighbouring proton core, enters its surface strain well, completes a half-orbit on the far side (where both protons pull inward, strengthening the anchor), then reaches the near side and detaches again — returning to the first core. At each crossing, the electron detaches from one core (beta decay) and is captured by the other (inverse beta decay), accompanied by a co-directional lattice wave (antineutrino). Inside the nucleus, every detachment is immediately followed by capture at the next core — a closed loop with no net particle emission. The "weak force" is what this continuous exchange looks like from outside when the loop breaks: in a free neutron, the electron detaches with no nearby core to catch it, and both the electron (beta particle) and lattice wave (antineutrino) escape to infinity.

The figure-8 electron screens approximately 50% of the proton–proton Coulomb repulsion, computed by time-averaging the net electromagnetic force over 720 electron positions around the full orbit. One electron cannot neutralise two protons — when the electron is on the far side of its current core, it pulls that core away from the other, adding to the repulsion. The near-side phases are attractive (approximately −1.0 MeV/fm), the far-side phases repulsive (+1.2 to +1.6 MeV/fm depending on core separation), and the time average is roughly 50% screening at all distances tested (2.0 to 5.0 fm).

For three proton cores (tritium, He-3), the topology changes. He-3 has one electron for three cores. One proposed orbit is a trefoil — the electron visiting all three cores in sequence, screening each edge for one-third of the period. Other topologies, such as a figure-8 between two of the three cores, would screen those two more effectively but the third less so. Regardless of the exact topology, He-3 is stable: it has the minimum possible electron count (one) for three cores, and removing it would leave three bare protons — no nucleus. Tritium has two electrons for three edges: two edges screened, one frustrated. The geometric frustration drives tritium's beta decay (half-life 12.3 years) — the frustrated electron eventually escapes, leaving He-3. The binding energy difference between tritium and He-3 (0.764 MeV) is a direct measurement of one electron's screening contribution.

 doi:10.20944/preprints202604.0421.v1

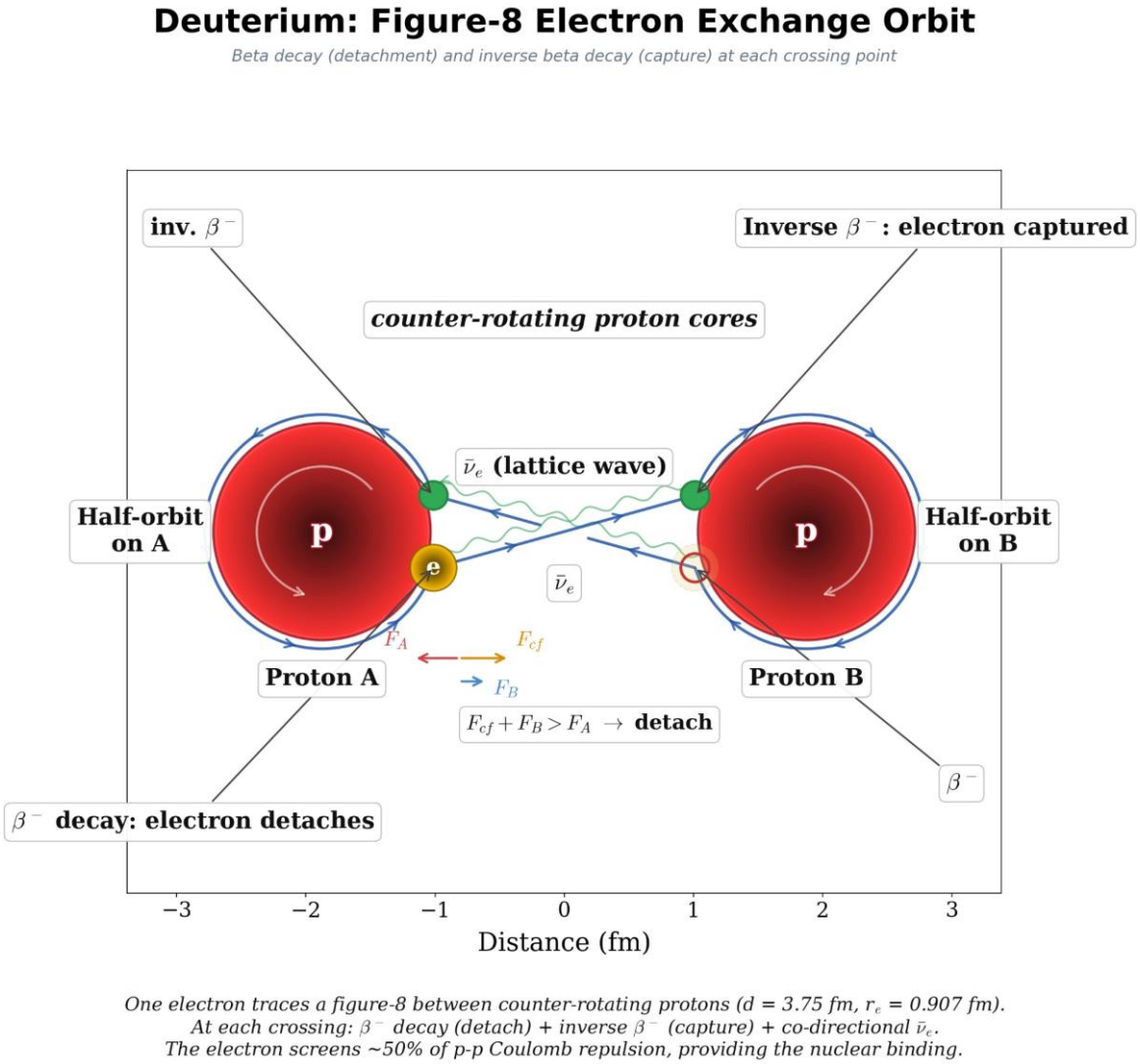

Figure 5. Deuterium: figure-8 electron exchange orbit. One electron (yellow) traces a shared path between two proton cores (red, d = 3.75 fm, r_e = 0.907 fm) whose spin axes are tilted at 109.47° (the tetrahedral angle between their respective sublattice directions). At each crossing point, the electron detaches from one core (β^- decay) and is captured by the other (inverse β^-), accompanied by a co-directional lattice wave (antineutrino, $\bar{\nu}$_e).

He-4, with four proton cores on a rock salt square and two electrons, achieves the most symmetric configuration: each electron traces a figure-8 along one diagonal, screening both diagonals simultaneously with the electrons maximally separated. No edge is frustrated. Every core is equivalent. This perfect coverage, combined with the strong-force binding from four mutual contacts, produces the highest binding energy per nucleon of any nucleus (7.07 MeV/A).

In nuclei larger than He-4, the electron does not simply turn around at each core. With multiple proton cores packed in rock salt ordering, the next core along the same [111] channel pulls the electron forward. The electron threads through the nuclear interior on an S-shaped path: half-orbit on one core's surface, detach, fly across the ~0.35 fm gap, capture at the next core, half-orbit on the opposite side, detach again — continuing until it reaches the nuclear surface. At the surface, with no forward core, the electron completes a full orbit before heading back along a different [111] channel. Surface nucleons that retain a complete electron orbit are what we observe as neutrons; interior cores, constantly flickering between bare and screened as electrons pass through, have no fixed proton or neutron identity. This is the physical origin of isospin symmetry — the experimental observation that protons and neutrons are nearly interchangeable inside nuclei.

 doi:10.20944/preprints202604.0421.v1

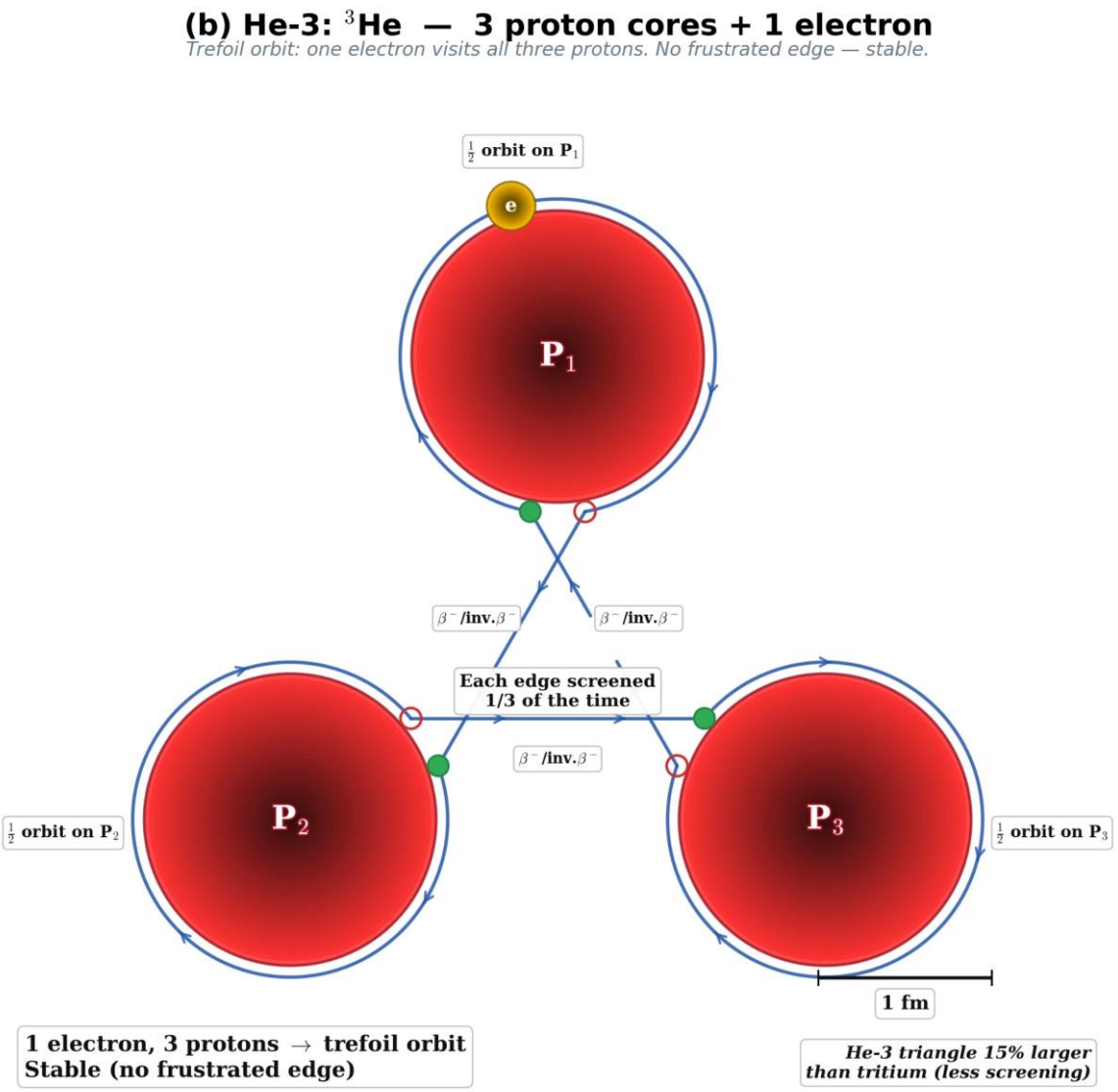

Figure 6. He-3: proposed trefoil electron orbit. One electron (yellow) shared among three proton cores (P_1, P_2, P_3). In the proposed topology, the electron visits all three cores in sequence, performing a half-orbit on each before detaching to the next (β^-/inverse β^- at each crossing), screening each edge for one-third of the orbital period. The He-3 triangle is 15% larger than tritium's (less screening → more Coulomb repulsion).

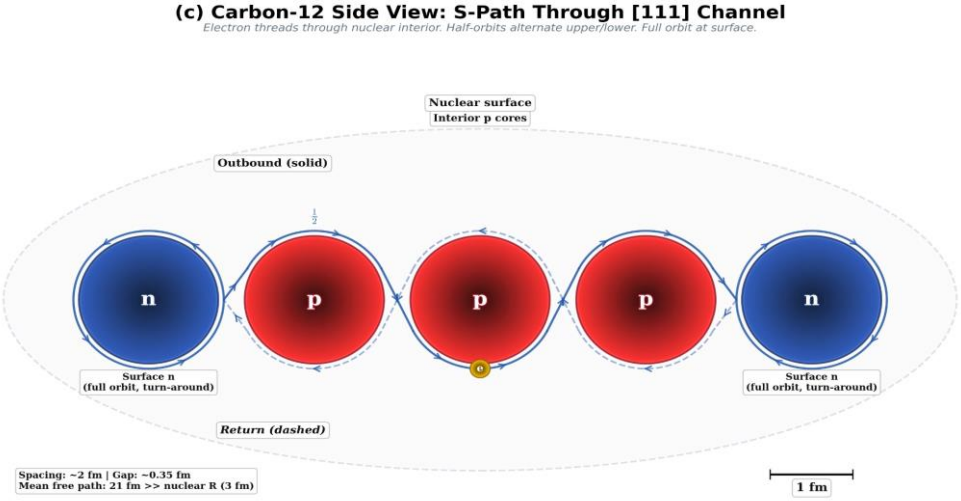

 doi:10.20944/preprints202604.0421.v1

Figure 7. Carbon-12: S-path through a [111] channel. One electron (yellow) threads through the nuclear interior, performing alternating half-orbits on successive proton cores (red). At each surface neutron (blue), the electron completes a full orbit before reversing along a different channel.

For any N = Z atom, the electrons split exactly in half: Z electrons orbit inside the nucleus between proton cores at ~2 fm spacing, providing ~MeV-scale screening, and Z electrons orbit outside the nucleus around it at ~50,000 fm spacing, forming ~eV-scale chemical bonds. Both sets do the same job — thread between positive centres and screen their mutual repulsion — at different distance scales. The deuteron, with its full electron complement, is the nuclear analogue of H_2: two proton cores sharing two electrons, one on a nuclear-scale figure-8 orbit (~2 fm, ~MeV binding) and one on an atomic-scale orbit (~50,000 fm, ~eV binding). The nuclear subsystem alone — two proton cores plus one shared electron — maps to H_2^+. The analogy is not perfect: the nuclear bond additionally has the strong force, which dominates the binding energy. At atomic distances, no strong force operates and the bond is purely electromagnetic.

6.3. Heavy Nuclei and Neutron Excess

In light nuclei (A ≤ 40), rock salt ordering gives a 1:1 proton-neutron ratio. In heavy nuclei, cumulative Coulomb repulsion between protons raises the energy of the interior. Extra neutrons attach to the nuclear surface as a neutral skin, reducing the Coulomb stress without disrupting the 1:1 rock salt core. Even for lead-208 (44 excess neutrons), the extra neutrons occupy only ~18% of the available core surface area — surface-only accommodation is geometrically sufficient through the entire periodic table. Ca-40 and Ca-48 have the same charge radius (3.478 vs 3.477 fm) despite 8 extra neutrons — confirming that the proton-neutron core stays the same size and the extra neutrons pack outside it.

7. Electromagnetism

7.1. Charge

The FCC ether lattice is not merely a static scaffold — it carries an inherent directionality. Every hyphon spins with directed angular momentum along its tetrahedral axis: not just a spin rate, but a vector. The four sublattices together create a consistent directional pattern throughout space — not bulk rotation, but a coherent angular momentum field. The ABC stacking of the FCC lattice adds a handedness — ABCABC and CBACBA are mirror images that cannot be superimposed. This directionality and chirality together are the reference against which all charge is defined.

Charge arises from lattice distortion — a disruption of the lattice's equilibrium that propagates outward as a 1/r strain field. Two fundamentally different structures produce charge. The proton is a ~1000-hyphon vortex with a counter-rotating positron crowdion on its surface (Section 5.2). The electron is a crowdion soliton that disrupts the surrounding lattice at every position along its path (Section 5.1). Both produce one unit of lattice distortion. The sign is determined by the direction of the distortion: the proton's crowdion counter-rotates with the vortex (+1e); the electron's mismatch pushes it outward (−1e). The positron (opposite-chirality crowdion) and antiproton (opposite spin direction) are their mirror images.

The electron and positron are created as a pair — equal and opposite lattice distortions that together leave the lattice unchanged. Their charges are equal by construction. The proton carries charge +1e because a positron crowdion counter-rotates on its surface. There is no half-unit of mismatch — one crowdion, one distortion, one unit of charge. This is why fractional charges do not exist as free particles.

Each charged particle creates a distortion pattern in the surrounding lattice that radiates outward as a 1/r field. When two particles create the same type of distortion, the patterns reinforce between them — the lattice stores more strain energy in the overlap, and the system lowers its energy by moving them apart. This is repulsion. When two particles create opposite distortions, the patterns

 doi:10.20944/preprints202604.0421.v1

cancel between them — the lattice relaxes in the gap, and the surrounding pressure pushes them together. This is attraction. No force carrier is needed — the lattice itself, seeking its minimum energy configuration, produces the force.

7.2. Magnetism

7.2.1. Magnetism as Moving Charge Distortion

A stationary charged particle creates a spherically symmetric distortion pattern in the lattice — the electric field (Section 7.1). When the particle moves, this distortion pattern moves with it. But the lattice is not instantaneous: the distortion at the old position fades as the lattice relaxes, while the distortion at the new position builds up as the lattice deforms. This creates an asymmetry — the distortion pattern of a moving charge is no longer purely radial. It acquires a circular component that wraps around the direction of motion. This circular component is the magnetic field. Magnetism is not a separate force — it is the lattice's response to charge distortion in transit. In standard physics this is well known: the magnetic field is the relativistic correction to the electric field for moving charges. In the lattice model the same result has a mechanical origin — the lattice cannot deform and relax instantaneously, so a moving source of distortion leaves a swirling wake.

7.2.2. Current-Carrying Wire

In a straight current-carrying wire, many electron crowdions propagate through the lattice in the same direction. Each moving distortion pattern creates a circular component that propagates outward (Section 7.2.1). The patterns from all electrons along the wire add coherently — they all swirl the same way around the wire. The combined circular distortion falls as $1/r$ (spreading over a circumference $2\pi r$), producing the magnetic field measured around any current-carrying conductor.

7.2.3. Magnetic Dipole

A single orbiting electron — or any current loop — creates a circular distortion from each segment of its path. From far away, opposite sides of the loop produce swirls that partially cancel. What survives is weaker and falls as $1/r^3$ — the magnetic dipole field. The magnetic moment of an atom is set by its electron's orbital plane and speed.

7.2.4. Permanent Magnets and Materials

A permanent magnet is a collection of atoms whose electron orbital planes are aligned. Their individual circular distortion patterns add coherently, producing a macroscopic magnetic field. In most materials the orbital planes are random and cancel — no net field. In ferromagnetic materials, the lattice coupling between neighbouring atoms' electron orbits allows an external magnetic field to align them. Soft magnetic materials reorient easily; hard magnetic materials resist reorientation but retain alignment once achieved. Above the Curie temperature, thermal vibration overwhelms the alignment and magnetism is lost.

7.2.5. Electromagnetic Induction

When a magnetic field changes — because a magnet moves or a current varies — the circular distortion pattern shifts through the lattice. Any electron in the path of this shifting pattern gets pushed by the changing lattice strain, producing a current. This is Faraday's law: changing magnetic flux induces an electromotive force. In the lattice model it is purely mechanical — a moving strain pattern pushes charges, just as a water wave pushes a floating object.

7.3. Lightning and Electrical Discharge

Lightning and electrical discharge occur when the charge distortion in the lattice exceeds a critical threshold. In normal conduction, electron excitations hop between hyphons one at a time,

 doi:10.20944/preprints202604.0421.v1

each hop requiring energy to overcome the lattice coupling barrier. The distortion field from a charge imbalance strains the lattice along the field direction, lowering this barrier. At sufficient field strength, the first electrons begin hopping through where the field is locally strongest. Their motion creates flow-like distortion along the path, which drops the local lattice pressure by the same Bernoulli mechanism that produces gravity (Section 4). Lower pressure means a slightly stretched lattice — weaker coupling between elements — and easier hopping. Each additional electron deepens the low-pressure channel, making the next hop easier still. Meanwhile, the circular magnetic distortion around the channel (Section 7.2.1) raises pressure outside, confining the low-pressure tube to a narrow path. The result is a self-reinforcing, self-focusing avalanche: a temporary vortex tube in the lattice with low pressure inside (easy conduction) and high pressure outside (barrier). The stepped leader observed in lightning is this avalanche propagating in stages — advancing where the field is strong, pausing where it weakens, building up distortion, then jumping again. Once the channel connects the charge reservoirs, the full imbalance discharges through the low-pressure path in microseconds (the return stroke). The rapidly changing current produces intense electromagnetic radiation because the hop pulses no longer cancel as they do in steady current. Once the charge imbalance equalises, the flow stops, pressure normalises, and the lattice relaxes to its ground state.

8. Chemistry

The chemical bond is the same electron-sharing mechanism operating at atomic distances without the strong force. Two atomic nuclei separated by ~1 Å share one or more electrons that thread through the hyphon lattice between them, screening their mutual Coulomb repulsion — precisely as nuclear electrons screen proton cores at ~2 fm.

9. Quantitative Predictions

The model produces a chain of calculations connecting FCC geometry to the fine structure constant $\alpha \approx 1/137$. The chain is: FCC frustration → torsional stiffness → Morse steepness → crowdion coupling g → electron mass → hyphon mass → α. The first-principles calculation gives α to within 11%; a single calibration parameter (g) closes the gap.

9.1. The Coupling Constant g

The electron is a crowdion — a kink soliton in the Frenkel-Kontorova model. Its mass relative to the hyphon mass is $m_e/m_h = 2/(\pi^2\sqrt{g})$, where g is the dimensionless ratio of in-row elastic coupling to off-row barrier height (Braun & Kivshar, 1998).

In FCC, each close-packed row atom has 12 nearest neighbours: 2 in-row ($\cos^2\theta = 1$), 8 at 60° ($\cos^2\theta = 1/4$), and 2 perpendicular ($\cos^2\theta = 0$). The total in-row stiffness ($2V''$) exactly equals the off-row restoring force ($8 \times V''/4 = 2V''$) — a geometric identity of 12-fold FCC coordination. This balance constrains g close to unity.

Computing g from first principles requires deriving the Morse steepness α_{Morse} from the lattice geometry. The chain is: (1) Spinning spheres in FCC cannot all mesh (frustration mismatch = 2/3 per bond, exact geometric result). (2) The mismatch creates a torsional interaction between neighbours, mediated by the inviscid fluid coupling between spinning spheres. (3) The wave speed constraint $v_{transverse} = c$ fixes the spin rate ω in terms of the torsional stiffness. (4) The torsional stiffness determines the bond depth D. (5) D and the equilibrium spacing give α_{Morse}.

The calculation proceeds as follows: the mismatch energy per bond (2/3, exact) determines the torsional interaction energy between neighbours via Monte Carlo integration of the Stokes dipole flow field between touching spinning spheres (interaction coefficient $C_{bond} \approx -0.185$). The transverse wave speed equation $v = c$ fixes the product ωR in terms of this torsional stiffness and the moment of inertia ($I = 2/5\ ma^2$ for solid spheres). The bond depth D then follows from $D = \frac{1}{2} \times k_{torsional} \times (2/3)^2$, and $\alpha_{Morse} = \sqrt{(2D\alpha^2/K)}$ closes the chain. The hyphon mass cancels exactly —

 doi:10.20944/preprints202604.0421.v1

α_Morse is a pure geometric number. The result is α_Morse ≈ 3.8. The full derivation with code is provided in the supplementary material.

To obtain g at a given α_Morse, a crowdion barrier is computed in a 3D FCC Morse lattice. An FCC supercell (typically 6^3 conventional cells, 864 atoms, periodic boundaries) is built with Morse pair interactions V(r) = D(e^{−2α(r−d)} − 2e^{−α(r−d)}). One extra atom is inserted into a close-packed [110] row. The total energy of the system is computed as a function of the extra atom's position u along the row, from u = 0 (on a lattice site) to u = 0.5d (midpoint between sites — the saddle point). At each position, all atoms except the crowdion row are relaxed to their minimum-energy positions using L-BFGS minimisation. The energy difference $\Delta E = E(u=0.5) - E(u=0)$ gives the on-site barrier height A. The in-row spring constant $K = 2D\alpha^2$ is computed directly from the Morse potential second derivative. The dimensionless coupling is then $g = K/(4\pi^2 A)$. Convergence was verified by increasing the supercell from 4^3 to 12^3 — the relaxed g changes by less than 0.1% beyond 6^3.

Crowdion simulation of 3D FCC Morse lattices gives the following g values: at α_Morse = 3.8, g = 0.81 and $1/\alpha = 152$ (+11% error); at 4.0, g = 0.89 and $1/\alpha = 145$ (+6%); at 4.2, g = 0.95 and $1/\alpha = 140$ (+2%); at 4.4, g = 1.01 and $1/\alpha = 136$ (−0.4%).

The first-principles value (α_Morse ≈ 3.8) gives g ≈ 0.81 and $1/\alpha = 152$, 11% above measured. The remaining gap traces to known approximations: the 1D chain dispersion used instead of the full 3D FCC dispersion relation, the solid-sphere assumption for the moment of inertia ($I = 2/5\ ma^2$, whereas fluid vortices likely have $I_{eff} < 0.4\ ma^2$), and finite simulation box size.

The dimensionless steepness α_Morse ≈ 4.4 needed to match α_EM lies between silver (4.26) and lead (4.42) in the experimental tabulation of FCC metals by Girifalco & Weizer (1959). The hyphon lattice has the same dimensionless potential shape as an ordinary FCC metal.

9.2. The Fine Structure Constant

The FK formula determines the hyphon mass from the electron mass:

$$m_h = m_e \times \pi^2 \sqrt{g} / 2$$

The first-principles value g = 0.81 (Section 9.1) gives m_h = 2.27 MeV and N = m_p/m_h = 413. The fine structure constant follows:

$$\alpha = e \times m_h / m_p = e / N = 2.718 / 413 = 0.00658$$

$1/\alpha = 152$, approximately 11% above measured. This is the same 11% gap as in Section 9.1 — the error enters through g and propagates identically to both the electron mass ratio and α. Closing the gap in g (from 0.81 to 0.998) closes both simultaneously. The required g = 0.998 corresponds to α_Morse ≈ 4.4, which lies between silver (4.26) and lead (4.42) in the experimental tabulation of FCC metals by Girifalco & Weizer (1959). The calibration is a 19% adjustment in g, comparable to the estimated uncertainty in the first-principles stiffness calculation.

With g = 0.998: m_h = 2.519 MeV, N = 372, and $1/\alpha = 137.0$ — matching the measured value to 0.11%. The mass ratio N = m_p/m_h = 372 is not a physical hyphon count — the proton contains approximately 1000 hyphons in a toroidal vortex (Section 5.2), of which 37% of the collective energy is excitation above the lattice ground state.

The cancellation is exact: substituting $m_h = m_e \times \pi^2\sqrt{g}/2$ into $\alpha = e \times m_h/m_p$ eliminates the hyphon mass entirely. What remains is $\alpha = e \times m_e \times \pi^2\sqrt{g}/(2 \times m_p)$ — only measured masses (m_e, m_p), the geometric factor π^2, the lattice coupling g, and Euler's number e = 2.71828. Why Euler's number appears in this relationship is not understood.

10. Acknowledgements and Invitation to Collaboration

This document presents the core framework of the theory, deliberately limited to the strongest and most defensible ideas. Many details have been omitted—not because they do not exist, but because they remain speculative and require further development.

 doi:10.20944/preprints202604.0421.v1

The author is not an expert in all the fields this theory touches—fluid dynamics, nuclear physics, general relativity, quantum mechanics, and cosmology each have deep bodies of knowledge that deserve more rigorous treatment than one individual can provide. Significant work remains: matching existing experimental formulas to this model, deriving the vortex pressure profiles from first principles, and creating fluid dynamics models or CFD simulations to produce a quantitative picture.

Collaboration with physicists, mathematicians, and computational scientists who find these ideas worth exploring would be greatly welcomed—whether in formalising the mathematics, identifying experimental tests, uncovering errors, or developing the many details that this framework leaves open.

References

Abbott, B. P. et al. [LIGO Scientific Collaboration and Virgo Collaboration] (2016). Observation of gravitational waves from a binary black hole merger. Physical Review Letters, 116(6), 061102.

Abrikosov, A. A. (1957). On the magnetic properties of superconductors of the second group. Soviet Physics JETP, 5(6), 1174–1182.

Bardeen, J., Cooper, L. N., & Schrieffer, J. R. (1957). Theory of superconductivity. Physical Review, 108(5), 1175–1204.

Bell, J. S. (1964). On the Einstein Podolsky Rosen paradox. Physics Physique Fizika, 1(3), 195–200.

Bonometti, T., & Magnaudet, J. (2006). Transition from spherical cap to toroidal bubbles. Physics of Fluids, 18(5), 052102.

Braun, O. M., & Kivshar, Y. S. (1998). Nonlinear dynamics of the Frenkel–Kontorova model. Physics Reports, 306(1–2), 1–108.

Clauser, J. F., Horne, M. A., Shimony, A., & Holt, R. A. (1969). Proposed experiment to test local hidden-variable theories. Physical Review Letters, 23(15), 880–884.

Cook, N. D. (1994). Nuclear binding energies in lattice models. Journal of Physics G, 20, 1907–1917.

Cook, N. D. (2010). Models of the Atomic Nucleus: Unification Through a Lattice of Nucleons (2nd ed.). Springer.

Cziráki, Á. (2023). Stability of nuclei based on the new proton and neutron model. Natural Science, 15(12), 289–299.

Dirac, P. A. M. (1951). Is there an aether? Nature, 168, 906–907.

Ekholdt, R. (2009). A soliton model of the electron with an internal nonlinearity cancelling the de Broglie–Bohm quantum potential. arXiv:0906.0598.

Feynman, R. P. (1955). Application of quantum mechanics to liquid helium. Progress in Low Temperature Physics, 1, 17–53.

Fizeau, H. (1851). Sur les hypothèses relatives à l'éther lumineux. Comptes Rendus de l'Académie des Sciences, 33, 349–355.

Fröhlich, H. (1954). Electrons in lattice fields. Advances in Physics, 3(11), 325–361.

Garai, J. (2003). The double tetrahedron structure of the nucleus. arXiv:nucl-th/0309035.

Galster, S., Klein, H., Moritz, J., Schmidt, K. H., Wegener, D., & Bleckwenn, J. (1971). Elastic electron-deuteron scattering and the electric neutron form factor at four-momentum transfers 5 $fm^{-2} < q^2 < 14$ fm^{-2}. Nuclear Physics B, 32(1), 221–237.

Girifalco, L. A., & Weizer, V. G. (1959). Application of the Morse Potential Function to Cubic Metals. Physical Review, 114(3), 687–690.

Hall, H. E., & Vinen, W. F. (1956). The rotation of liquid helium II: The theory of mutual friction in uniformly rotating helium II. Proceedings of the Royal Society A, 238(1213), 215–234.

Hill, M. J. M. (1894). On a spherical vortex. Philosophical Transactions of the Royal Society of London A, 185, 213–245.

Hoek, M. (1868). Determination de la vitesse avec laquelle est entraîné un rayon lumineux. Archives Néerlandaises des Sciences Exactes et Naturelles, 3, 180–185.

Kestler, M. F., Woo, K. C., Lim, J. W. X., Prins, L. M., Feldmann, J., & Loh, Z.-H. (2026). Direct observation of Fröhlich polaron formation in BiOI nanoplatelets. Physical Review Materials, 10, L022401.

 doi:10.20944/preprints202604.0421.v1

Landau, L. D. (1933). Über die Bewegung der Elektronen im Kristallgitter. Physikalische Zeitschrift der Sowjetunion, 3, 664–665.

Lorentz, H. A. (1892). La théorie électromagnétique de Maxwell et son application aux corps mouvants. Archives Néerlandaises des Sciences Exactes et Naturelles, 25, 363–552.

Lorentz, H. A. (1904). Electromagnetic phenomena in a system moving with any velocity smaller than that of light. Proceedings of the Royal Netherlands Academy of Arts and Sciences, 6, 809–831.

Maxwell, J. C. (1865). A dynamical theory of the electromagnetic field. Philosophical Transactions of the Royal Society of London, 155, 459–512.

Marjaneh, A. M., Saadatmand, D., Dmitriev, S. V., Gumerov, A., & Korznikova, E. A. (2018). Mass transfer in the Frenkel-Kontorova chain initiated by molecule impact. Physical Review E, 98, 023003.

Michelson, A. A., & Morley, E. W. (1886). Influence of motion of the medium on the velocity of light. American Journal of Science, 31(185), 377–386.

Michelson, A. A., & Morley, E. W. (1887). On the relative motion of the Earth and the luminiferous ether. American Journal of Science, 34(203), 333–345.

Miller, D. C. (1933). The ether-drift experiment and the determination of the absolute motion of the Earth. Reviews of Modern Physics, 5(3), 203–242.

Pohl, R. et al. (2010). The size of the proton. Nature, 466(7303), 213–216.

Shapiro, I. I. (1964). Fourth test of general relativity. Physical Review Letters, 13(26), 789–791.

Shepelev, I. A., Dmitriev, S. V., & Korznikova, E. A. (2023). Simulation of the dynamics of supersonic N-crowdions in fcc lead and nickel. Dynamics, 3(3), 44.

Sinha, K. P., Sivaram, C., & Sudarshan, E. C. G. (1976). Aether as a superfluid state of particle-antiparticle pairs. Foundations of Physics, 6(1), 65–70.

Veltmann, W. (1870). Über die Fortpflanzung des Lichtes in bewegten Medien. Annalen der Physik, 217(10), 497–504.

van Damme, R., Coli, G. M., van Roij, R., & Dijkstra, M. (2018). Revealing a vacancy analog of the crowdion interstitial in simple cubic crystals. Physical Review Letters, 121, 258001.

Volovik, G. E. (2003). The Universe in a Helium Droplet. Oxford University Press.

Yarmchuk, E. J., Gordon, M. J. V., & Packard, R. E. (1979). Observation of stationary vortex arrays in rotating superfluid helium. Physical Review Letters, 43(3), 214–217.

Zeeman, P. (1914–1920). Fresnel's coefficient for light of different colours. Proceedings of the Royal Academy Amsterdam, 17–22 (multiple papers).

Zloshchastiev, K. G. (2011). Spontaneous symmetry breaking and mass generation as built-in phenomena in logarithmic nonlinear quantum theory. Acta Physica Polonica B, 42(2), 261–292.